Accretion Disks, Jets and Winds: Theory and Simulations

A. MIGNONE
DIPARTIMENTO DI FISICA
UNIVESRITÀ DI TORINO (ITALY)

Outline

1. General overview in accretion physics: open problems;
2. The MagnetoRotational Instability (MRI)
3. Local Disk Models: shearing box
4. Global Disk Models
5. Magnetically Driven Outflows
6. Morphology and Propagation of Jets

Part 1: General Overview

Accretion Physics

- *Accretion disk*

  structure of gas in orbital motion around a central object (typically newborn star, neutron star, supermassive black hole);

- *Jet*

  collimated outflow emerging from the innermost regions of an accretion disk.

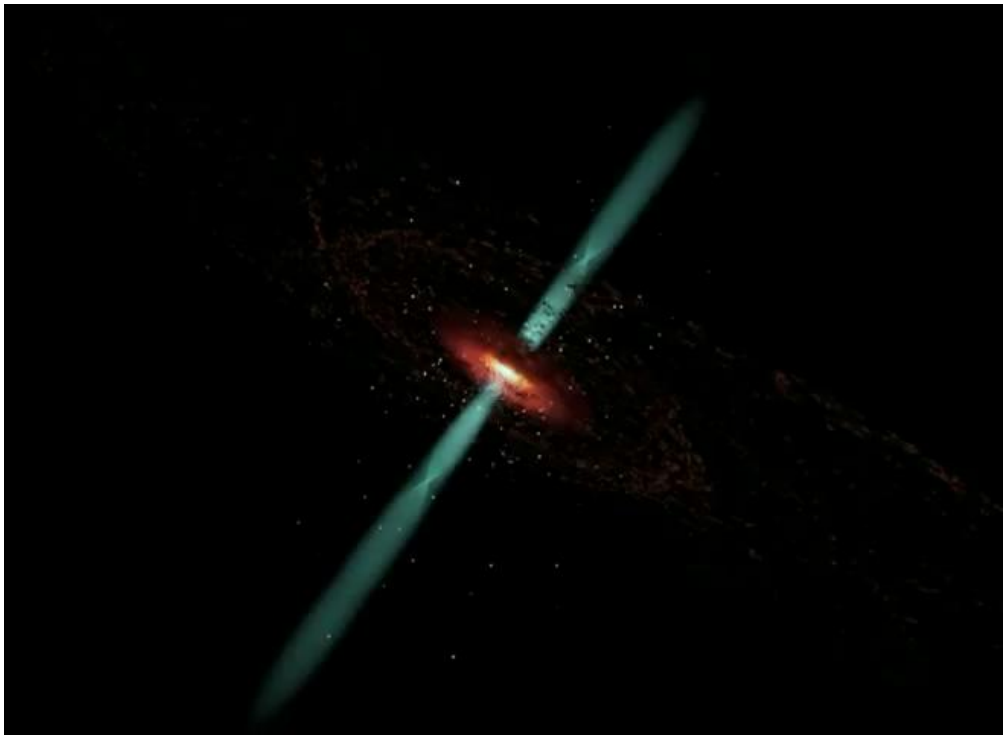

What is their connection ?

Accretion/Ejection systems

Star Formation Regions / Young Stellar Objects (YSO)

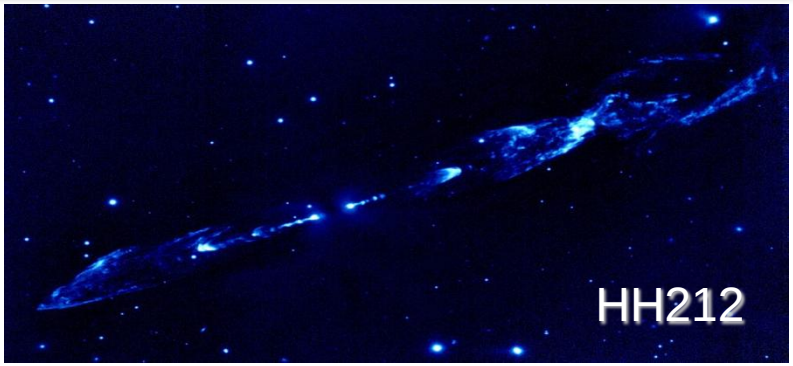

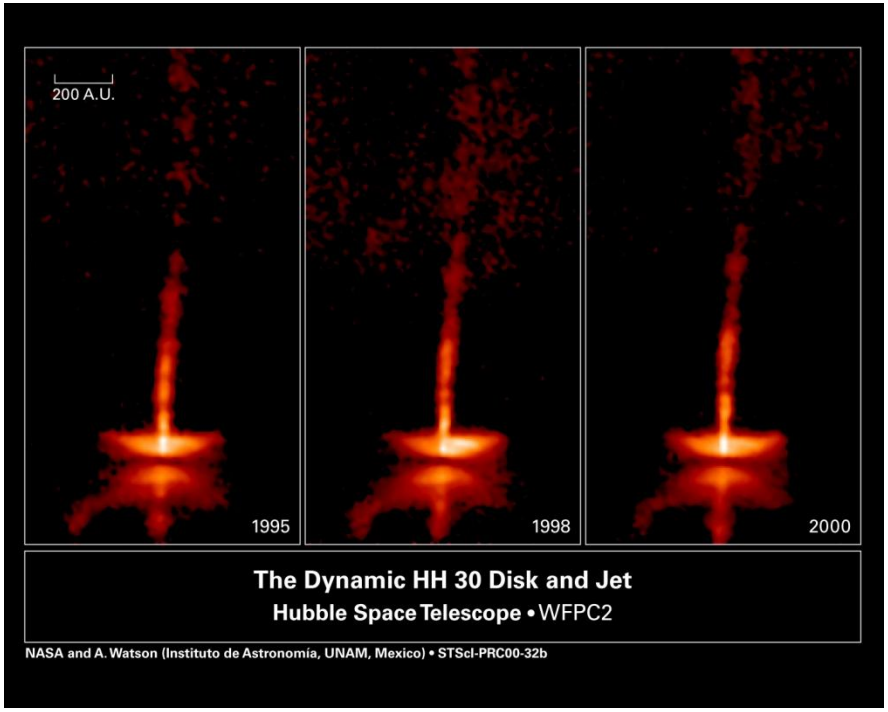

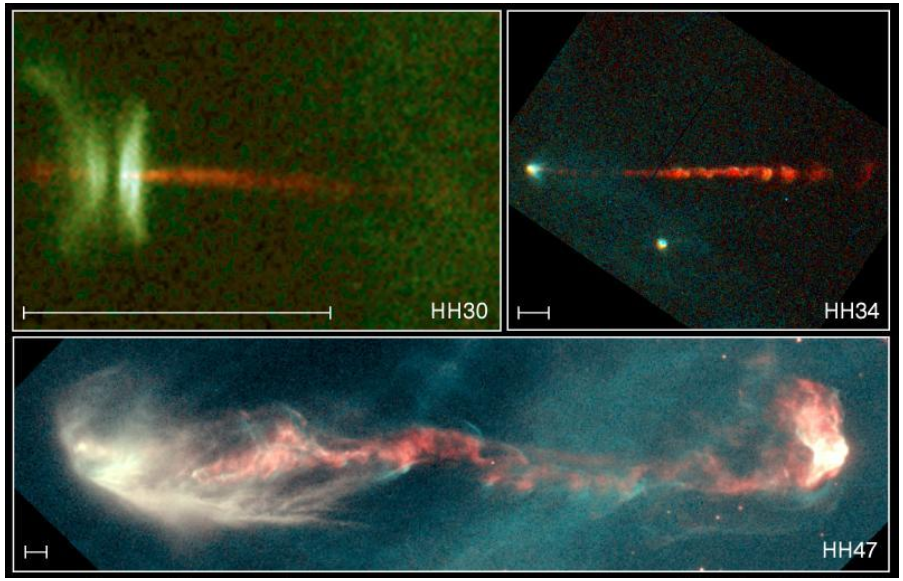

vel ~100–500 km/s; n~10^3–10^4 cm^{-3}; Size~10^3–10^5 AU; T~10^3–10^4 K; Age: 10^4–10^5 yrs

Thermal emission processes

Accretion/Ejection systems

Compact Objects (BH, NS)

X-Ray Binaries

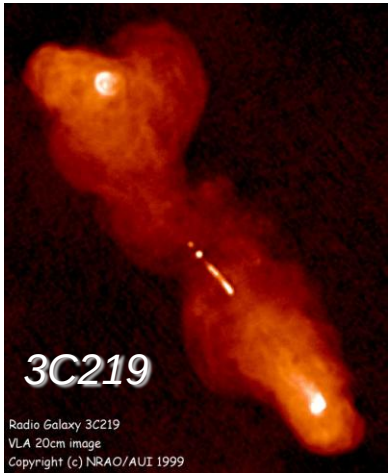

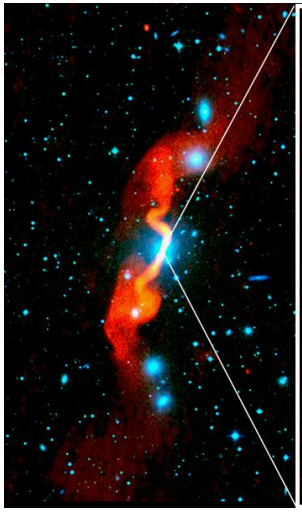

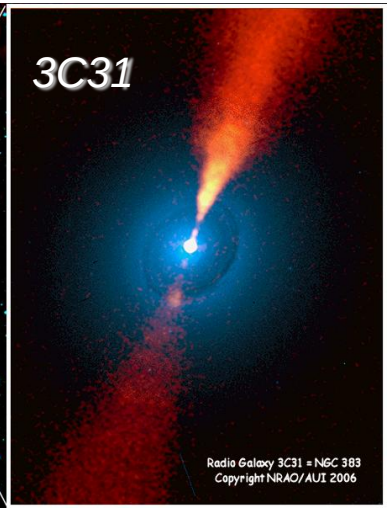

Micro Quasars

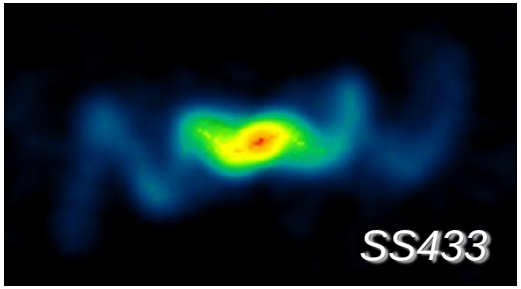

Active Galactic Nuclei (AGN)

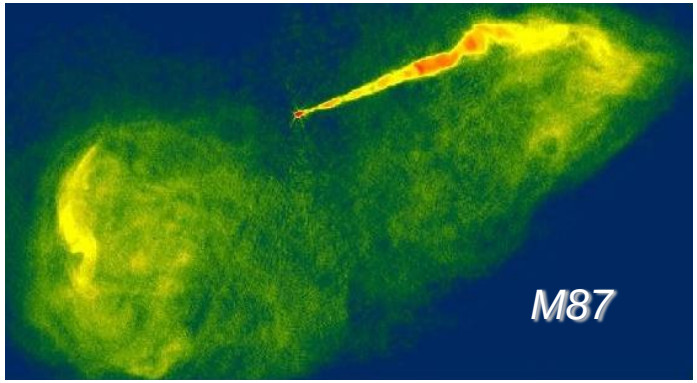

Vel~10^{-2}-1 c; n~10^{-5}-10^{-3} cm $^{-3}$; Size ~ few kpc–Mpc; Age~10^{7}-10^{8} yrs;

Non-thermal emission processes

Accretion Disks: Open Problems

- Accretion disks form because gas falling onto a gravitating object inevitably has some angular momentum (a.m.) that forces it to orbit around the object;

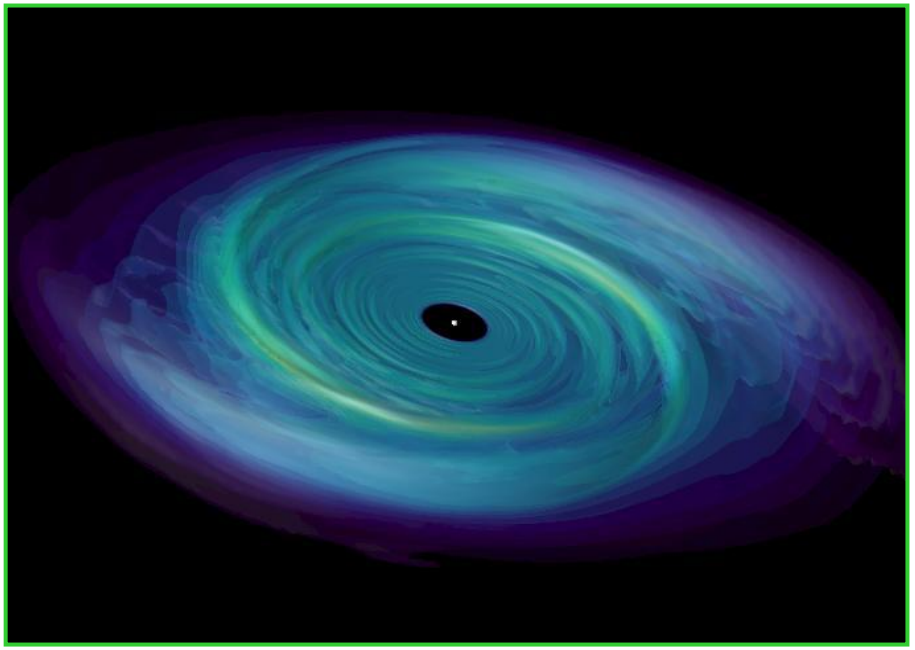

- Gravity causes material to spiral inward towards the central body only if a.m. is transported outwards;

- Infalling matter must loose gravitational energy and momentum: Angular momentum extraction at the origin of the jet paradigm.

Accretion Disks: Open Problems

- Turbulence possible source of angular momentum transport in accretion disks[1];

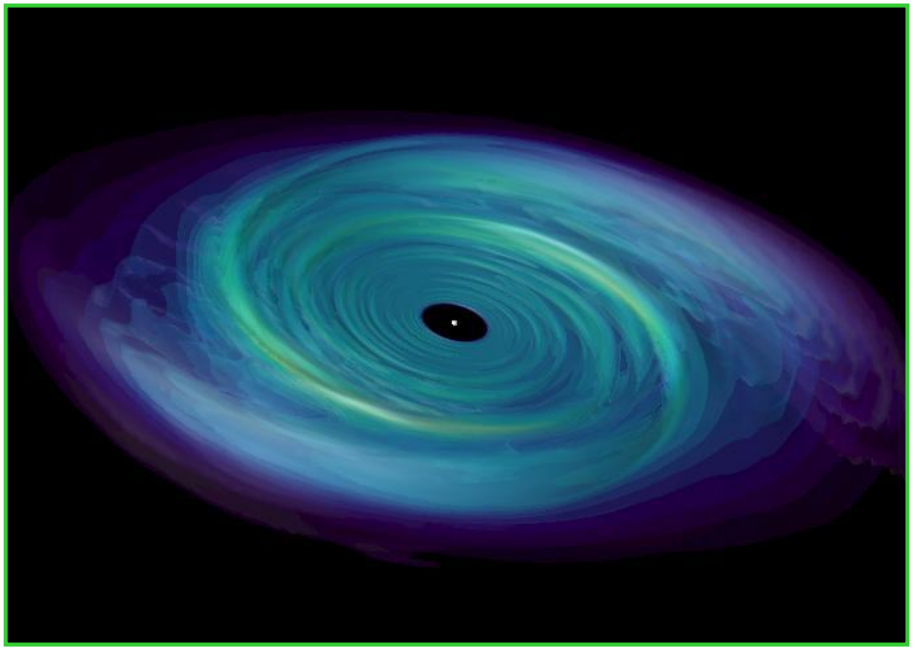

- Problem: microscopic viscosity not sufficient
  → turbulent enhanced viscosity
  → what is its origin ?

- Magnetorotational instability (MRI[2,3]) re-discovered by Balbus & Hawley (1991) proposed as the main process at the base of angular momentum transport in accretion disks.

[1]Shakura & Sunyaev, 1973; [2]Velikhov 1959; [3]Chandrasekhar 1960; [4]Balbus & Hawley (1990)

PART #2:
The Magnetorotational Instability (MRI)

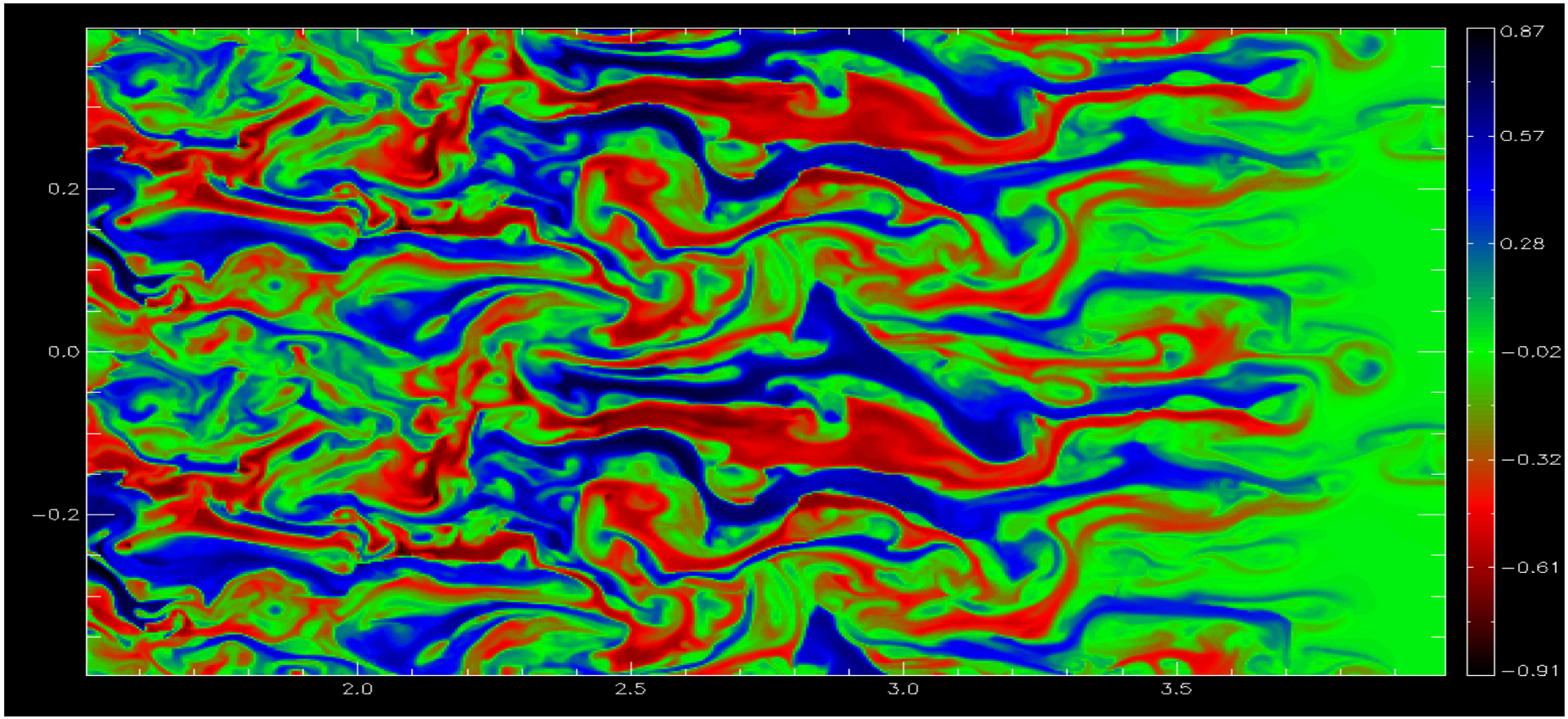

The MRI: Basic Principles

- MRI is a fluid instability whereby fluid elements exchange angular momentum via distorted field lines;
- It is an intrinsic MHD instability acting in differentially rotating magnetized disks;
- It works for weak magnetic fields ($\beta > 1$);
- The MRI leads to MHD turbulence and provides the necessary physical mechanism to remove angular momentum and allow accretion onto the central object.

The MRI: Basic Principles

- In cylindrical coordinates (R, ϕ, z), consider a disk rotating around a central object with mass M and threaded by a vertical magnetic field $\boldsymbol{B} = B_0 \boldsymbol{e}_z$.

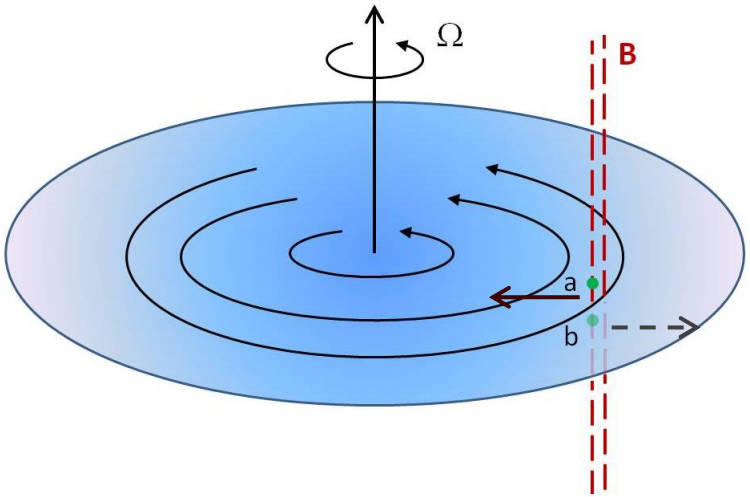

- Consider two fluid elements lying on the same vertical field line “a” and “b”: magnetic field acts as a “spring” connecting two neighboring fluid elements.
- Now perturb the field line in such a way that element “a” shifts at lower radii while element “b” shifts at larger radii.

The MRI: Basic Principles

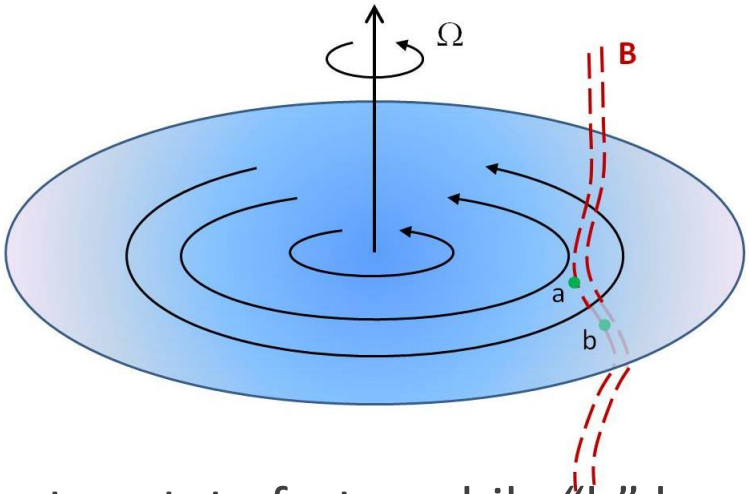

- Since $R_a < R_b$, "a" has to rotate faster while "b" has to slow down.
- Meanwhile, the line stretches and develops tension so as to slow down "a" and accelerate "b".
- During this process, "a" looses its angular momentum and drops down to yet smaller radii to accommodate its reduced angular momentum while "b" shifts to yet larger radius.
- The perturbation grows further and the process runs away.

The MRI: Linear Analysis

- Consider the (incompressible) MHD equations in (R, ϕ, z) coords:

$$\begin{aligned}
\rho\left(\frac{\partial v_R}{\partial t}+\boldsymbol{v}\cdot\nabla v_R\right)-\boldsymbol{B}\cdot\nabla B_R+\frac{\partial}{\partial R}\left(p+\frac{\boldsymbol{B}^2}{2}\right) &= \rho\left(\frac{v_\phi^2}{R}+g_R\right)-\frac{B_\phi^2}{R}\\
\rho\left(\frac{\partial v_\phi}{\partial t}+\boldsymbol{v}\cdot\nabla v_\phi\right)-\boldsymbol{B}\cdot\nabla B_\phi &= -\frac{B_\phi B_R}{R}\\
\rho\left(\frac{\partial v_z}{\partial t}+\boldsymbol{v}\cdot\nabla v_z\right)-\boldsymbol{B}\cdot\nabla B_z+\frac{\partial}{\partial z}\left(p+\frac{\boldsymbol{B}^2}{2}\right) &= 0\\
\frac{\partial \boldsymbol{B}}{\partial t}-\nabla\times\left(\boldsymbol{v}\times\boldsymbol{B}\right) &= \boldsymbol{0}
\end{aligned}$$

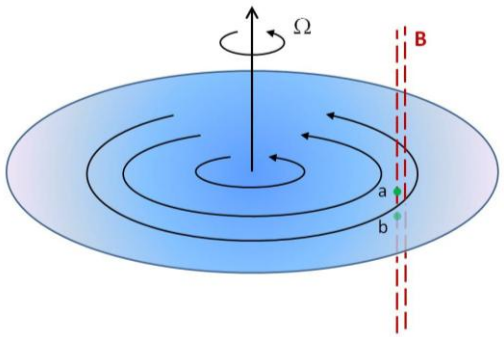

- In equilibrium, gravity is balanced by centrifugal term:

$$g_R = -GM/R^2 \equiv -R\Omega^2(R)$$

and a uniform vertical field $\boldsymbol{B} = B_0\boldsymbol{e}_z$ does not alter the equilibrium.

The MRI: Linear Analysis

- Introducing a perturbation $\delta \boldsymbol{v} = (\delta v_R, \delta v_\phi, 0)$ from the induction equation one obtains

$$\delta \boldsymbol{B} = B_0 ik \boldsymbol{\xi} \quad \longrightarrow \quad \frac{ikB_0}{4\pi\rho_0}\delta \boldsymbol{B} = -\left(\boldsymbol{k}\cdot\boldsymbol{v_A}\right)^2 \boldsymbol{\xi}$$

with $\boldsymbol{v}_A = \boldsymbol{B}_0/(4\pi\sqrt{\rho})$, the form of a spring-like force, linearly proportional to the displacement $\boldsymbol{\xi} = \int \boldsymbol{v}\, dt$.

- In a frame corotating with a small patch of the disk at R_0, the acceleration term in the momentum equation becomes

$$\frac{v_\phi^2}{R} + 2\Omega_0 v_\phi + R\Omega_0^2 - R\Omega^2(R) \approx 2\Omega_0 v_\phi - xR\frac{d\Omega^2}{dR}$$

where $x = R - R_0 \ll R_0$, and O(1/R) terms have been neglected.

The MRI: Linear Analysis

- The equations of motion take the form

$$\begin{cases} \ddot{x} &= 2\Omega_0 \dot{y} - xR\dfrac{d\Omega^2}{dR} - (\boldsymbol{k}\cdot\boldsymbol{v}_A)^2 x \\ \ddot{y} &= -2\Omega_0 \dot{x} - (\boldsymbol{k}\cdot\boldsymbol{v}_A)^2 y \end{cases}$$

- A solution with $x,y \propto e^{-i\omega t}$ possible if the dispersion relation holds:

$$\omega^4 - \omega^2\left[\kappa^2 + 2(\boldsymbol{k}\cdot\boldsymbol{v}_A)^2\right] + (\boldsymbol{k}\cdot\boldsymbol{v}_A)^2\left[(\boldsymbol{k}\cdot\boldsymbol{v}_A)^2 + \frac{d\Omega^2}{d\log R}\right] = 0$$

where $\kappa^2 = 4\Omega^2 + d\Omega^2/d\log R$ is the epicyclic frequency.

- The condition for stability ($\omega^2 > 0$) leads to $\dfrac{d\Omega^2}{dR} \geq 0 \quad \text{(Stability)}$

- In astrophysical disks, this is almost *never true*.

The MRI: Linear Analysis

- In a Keplerian disk $\Omega \propto R^{-3/2}$ and the previous criterion does not hold → instability.
- In this case, the maximum growth rate is found for

$$|\omega_{\max}| = \frac{1}{2}\left|\frac{d\Omega}{d\log R}\right| \qquad (\boldsymbol{k}\cdot\boldsymbol{v}_A)^2_{\max} = -\left(\frac{1}{4}+\frac{\kappa^2}{16\Omega^2}\right)\left|\frac{d\Omega^2}{d\log R}\right|$$

- Which, for a Keplerian disk become

$$|\omega_{\max}| = \frac{3}{4}\Omega\,, \qquad (\boldsymbol{k}\cdot\boldsymbol{v}_A)_{\max} = \frac{\sqrt{15}}{4}\Omega$$

- An enormous growth rate!

Example: 2D Axisymmetric Disk[1]

- Initial configuration enters in the nonlinear stage
- Ensuing of MHD turbulence
- Issues with inner boundary condition

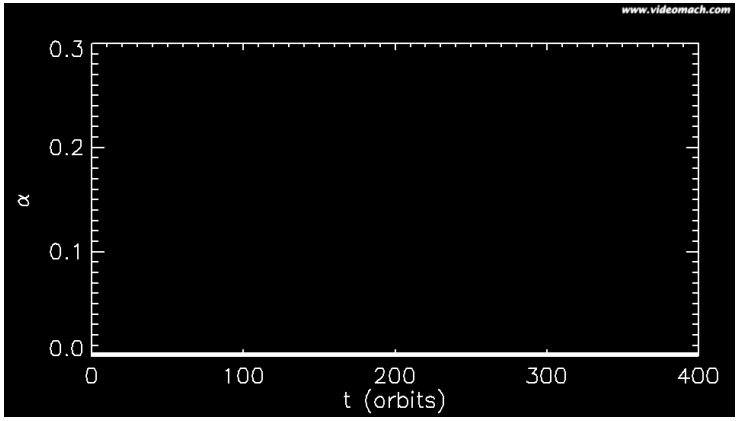

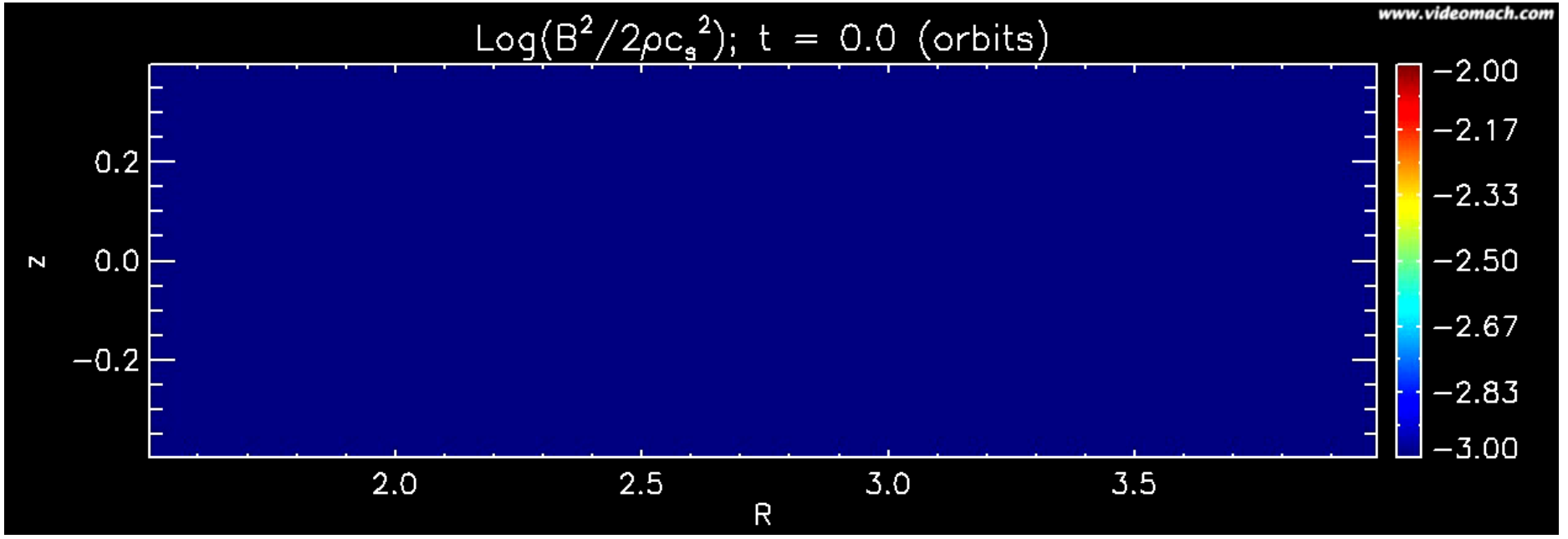

[1]PLUTO source files available on school website.

Accretion Disk Models

Local Models

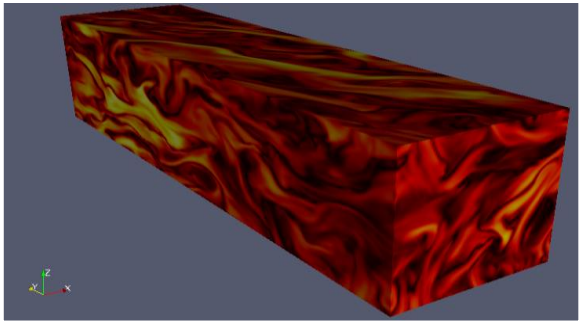

- Focus on a small disk patch;
- allow to reach larger resolutions;
- meaningful if they capture the characteristic of the MRI driven turbulence and AM transport.

Global Models:

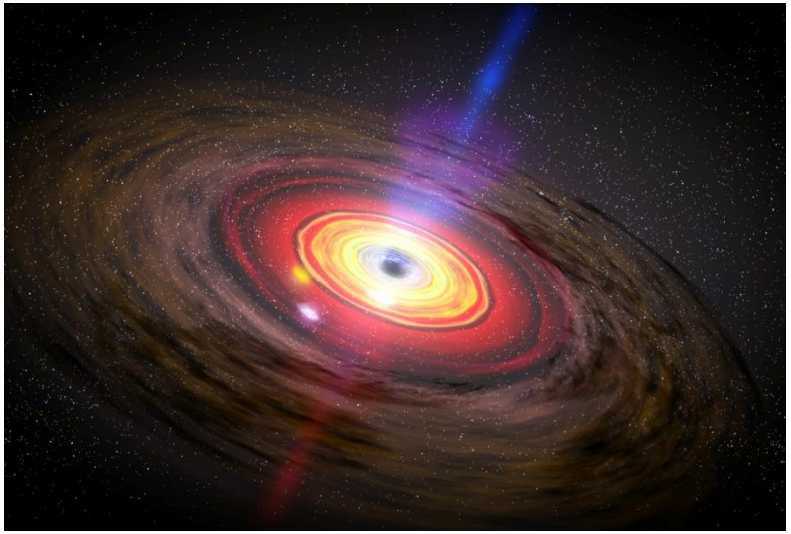

- More complete description of a real disk;
- extremely challenging for modern supercomputers ($\gg 10^7$ CPU hours)
- Issues with radial and vertical boundary conditions.

PART #3:
Local Models of Accretion Disks

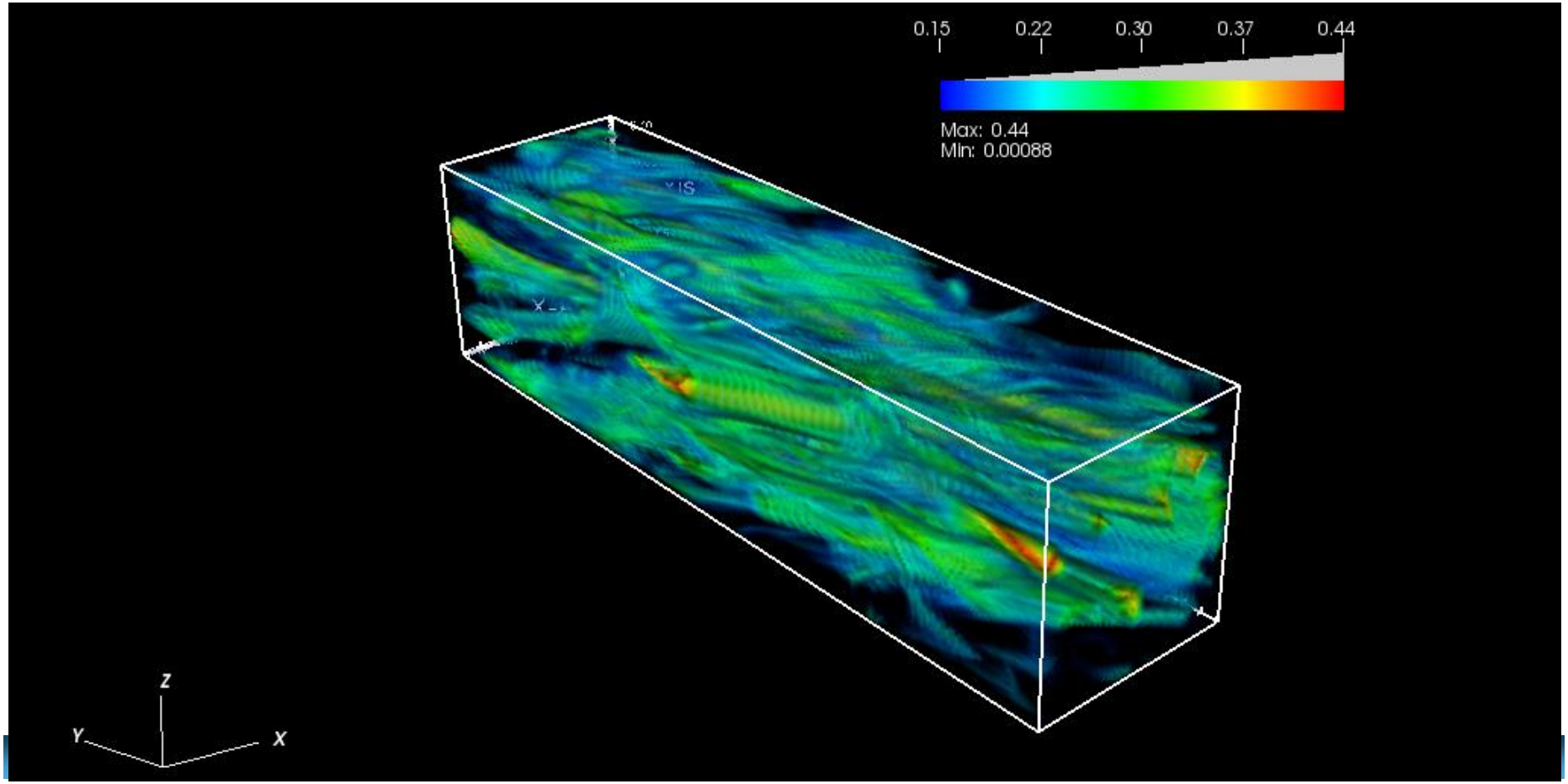

Local Models: The Shearing Box Approximation

- Much of what is presently known about MRI comes from numerical simulations using the shearing box approximation (SBA).
- The SBA is a local model of a differentially rotating disk based on a local expansion of the tidal forces in a reference frame corotating with the disk at some fiducial radius R_0.

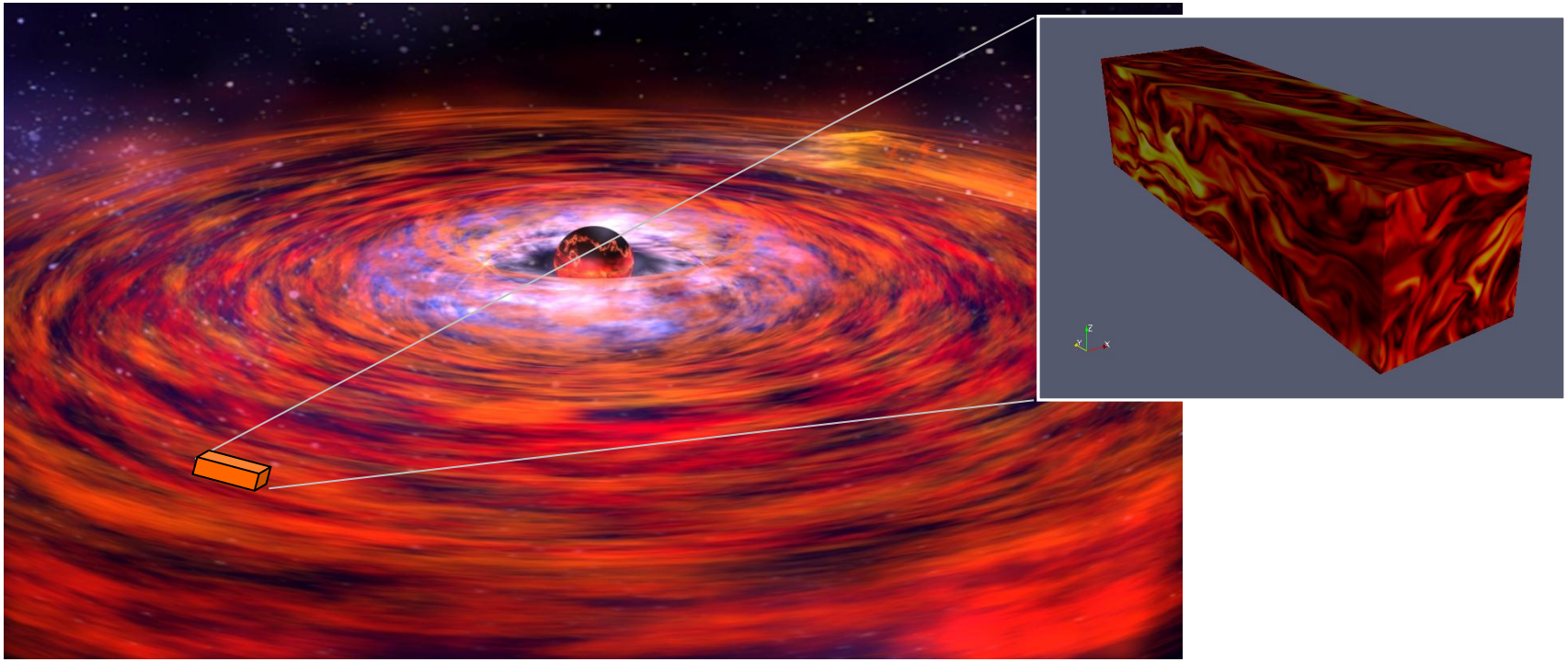

Shearing Sheet Equations

- If the box is sufficently small, curvature terms can be neglected and a local system of Cartesian coordinates is adopted:

  $(r - r_0) \rightarrow x$, $\phi \rightarrow y$, $z \rightarrow z$:

$$\frac{\partial \mathbf{v}}{\partial t} + \mathbf{v} \cdot \nabla \mathbf{v} + \mathbf{2\Omega} \times \mathbf{v} = \frac{\mathbf{B} \cdot \nabla \mathbf{B}}{4\pi\rho} - \frac{1}{\rho}\nabla\left(\frac{\mathbf{B^2}}{\mathbf{8\pi}} + \mathbf{p}\right) - \nabla\left(\mathbf{2A\Omega x^2} + \frac{\mathbf{1}}{\mathbf{2}}\mathbf{\Omega^2 z^2}\right)$$

- Where $A = \frac{R}{2}\left(\frac{\partial \Omega(R)}{\partial R}\right)_{R_0}$ is the shear rate.

- Keplerian profile: $A = -\frac{3}{4}\Omega$

- Velocity profile: $v_{y0} = -2Ax$

The Shearing Box Approximation

- Validity of the approximation restricted to a small Cartesian box with a steady flow consisting of a linear shear velocity, normally considered as the basic flow.

- While the computational box is periodic in the azimuthal (y) and vertical (z) directions, radial (x) boundary conditions are determined by “image” boxes sliding relative to the computational domain.

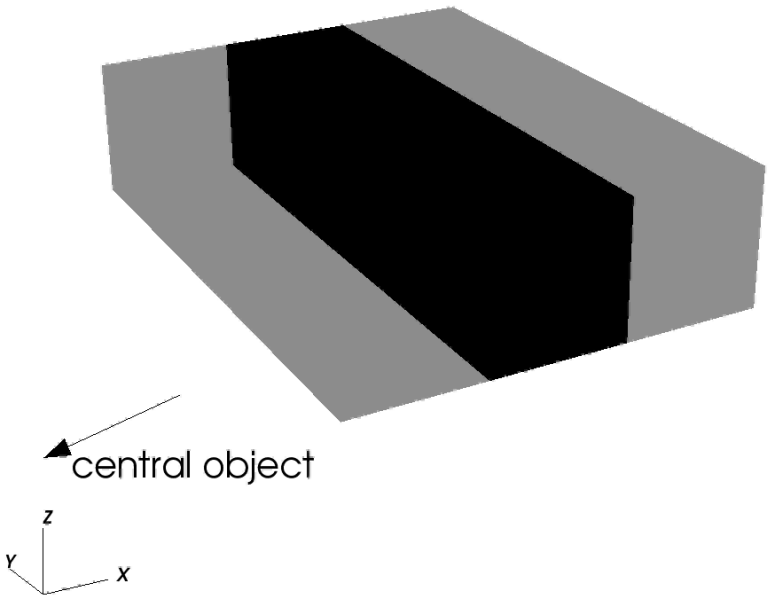

Boundary Conditions

- Vertical (z) direction:
  periodic/outflow/userdef
- Azimuthal (y) direction:
  periodic
- Radial (x) direction:
  Shearing boundary

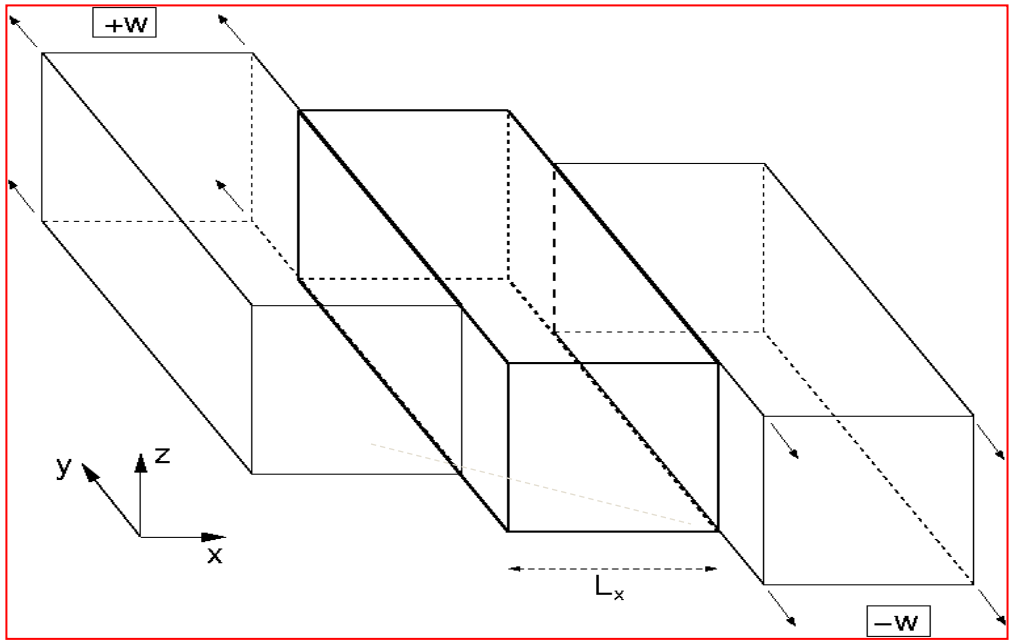

$$\begin{aligned} q(x,y,t) &= q\left(x+L_x, y-wt, t\right) \\ v_y(x,y,t) &= v_y\left(x+L_x, y-wt, t\right)+w \end{aligned}$$

left

$$\begin{aligned} q(x,y,t) &= q\left(x-L_x, y+wt, t\right) \\ v_y(x,y,t) &= v_y\left(x-L_x, y+wt, t\right)-w \end{aligned}$$

right

Numerical Issues

- By exploiting the periodicity in the y- and z- directions, volume-integrated quantities should be "conserved" under advection:

$$\int \left(\frac{\partial Q}{\partial t} + \nabla \cdot \vec{F} \right) d^3x = 0 \quad \Longrightarrow \quad \Delta\mathcal{V} \frac{d\langle Q \rangle}{dt} = \int \left[F_x(x_L, y, z) - F_x(x_R, y, z) \right] dy\, dz$$

- Strict conservation applies only to mass, z-momentum, x and z component of the magnetic field. For the y-component of B, the following relation must be satisfied:

$$\Delta\mathcal{V} \frac{d\langle B_y \rangle}{dt} = w \int B_x(x_L, y, z)\, dy\, dz \equiv w \int B_x(x_R, y, z)\, dy\, dz$$

- However, since the numerical fluxes are nonlinear functions of the Q's, truncation errors introduced by the interpolation algorithm in the radial ghost zones can lead to significant deviations from conservation.

Remapping Procedure

- Loss of conservation can be avoided by properly matching computed x-fluxes at the sheared domain boundaries:

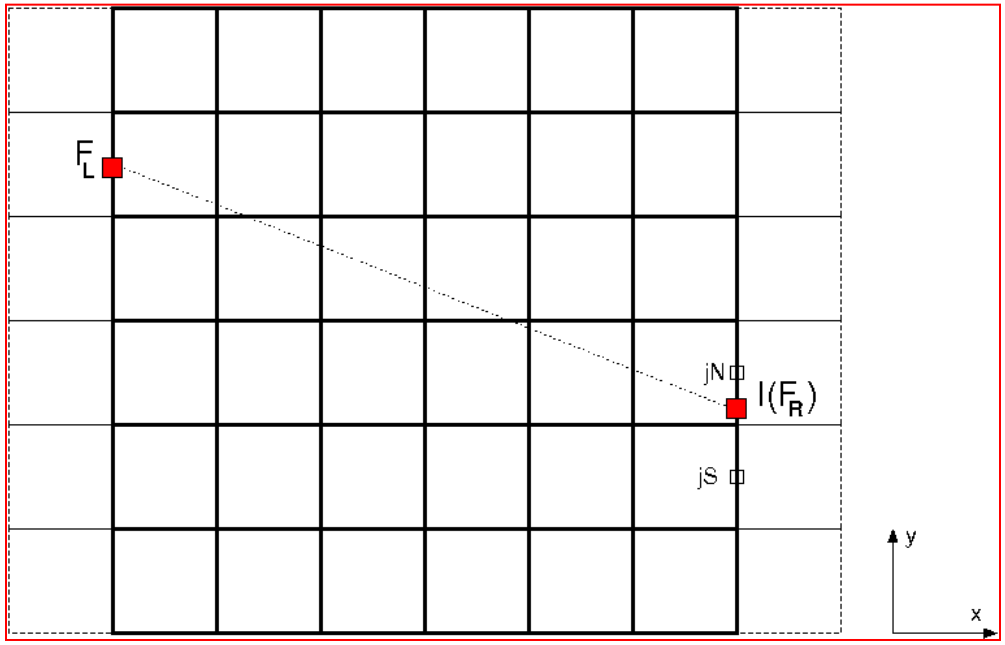

Fluxes not containing the azimuthal velocity (vy) are easily symmetrized by

$$F_L \rightarrow \frac{1}{2}\left[F_L + \mathcal{I}\left(F_R\right)\right] , \quad F_R \rightarrow \frac{1}{2}\left[F_R + \mathcal{I}\left(F_L\right)\right]$$

Ziegler (2007)

- Additional care is taken to ensure magnetic flux conservation by suitable remapping of the E.M.F z-component.

Remapping Procedure

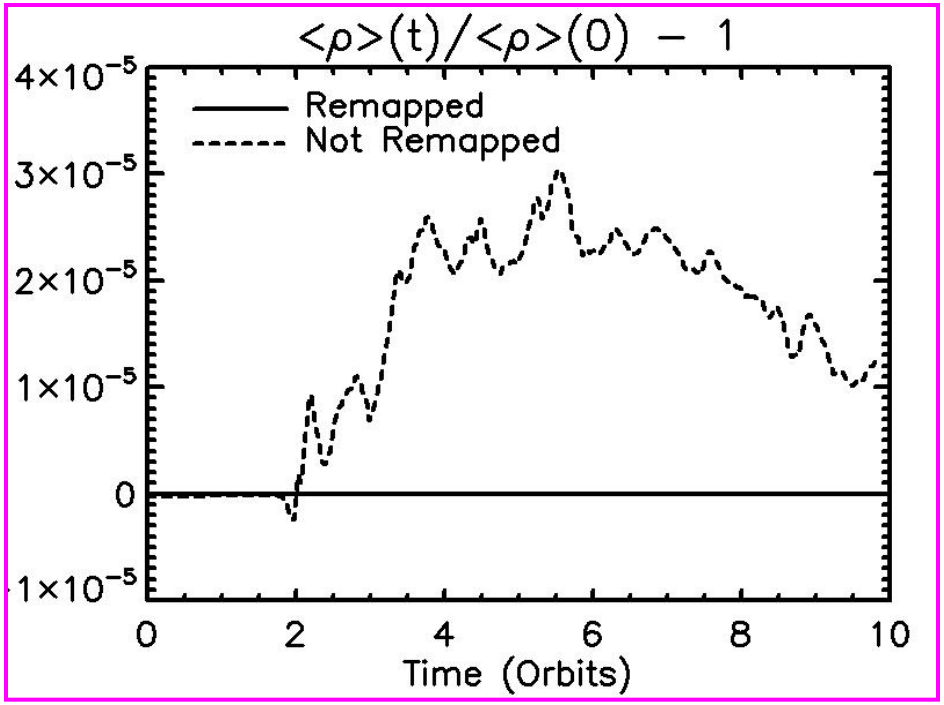

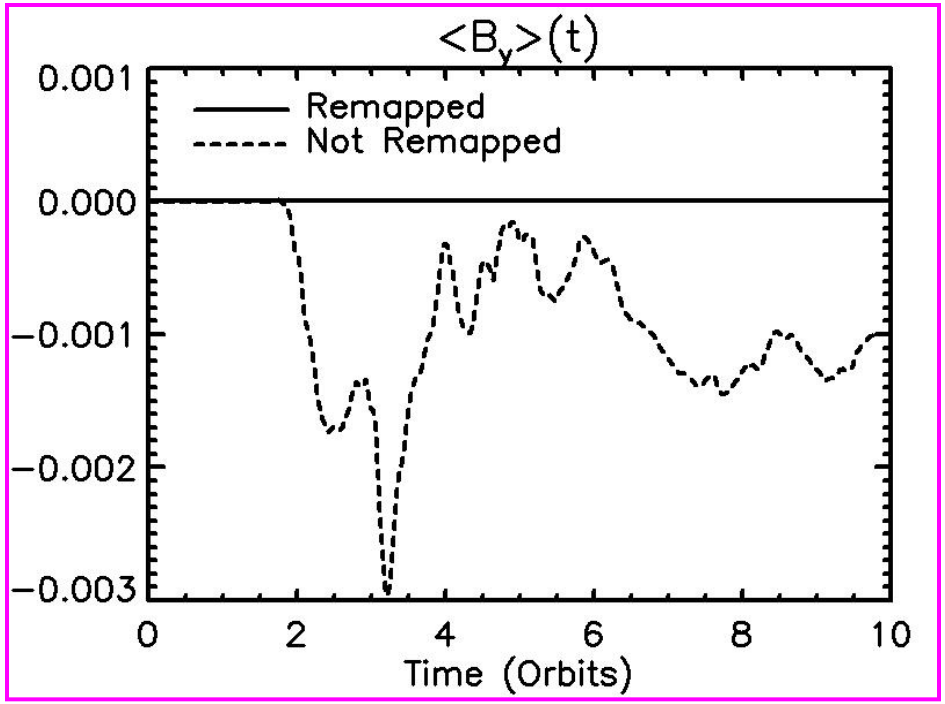

Exact Nonlinear MRI mode

- Goodman & Xu (1994) showed the existence of exact exponentially growing solutions of shearing sheet incompressible equations (channel solutions):

$$(B_x, B_y, B_z) = \epsilon B_0 \exp(st) \cos(Kz)(\sin\gamma, -\cos\gamma, 0) + (0, 0, B_0)$$

$$(v_x, v_y, v_z) = \epsilon v_0 \exp(st) \sin(Kz)(\cos\gamma, \sin\gamma, 0) + (0, 2Ax, 0)$$

- K: wave number (K ∥ rotation axis),
- γ: angle between the magnetic field and the y direction
- B_0 background axial field, $v_0 = -2A/K \sin 2\gamma$

- Velocity and magnetic field fluctuations are orthogonal;

- growth rate $s = -A \sin(2\gamma)$

Exact Nonlinear MRI mode

- $s > 0$ → exponentially growing solutions
- $\gamma = \pi/2$ (radial field), $s = 0$
- Fastest growing mode has $\gamma = \pi/4$, $K \approx \Omega/V_A$
- The nonlinear exact mode is itself linearly unstable to secondary "parasitic" instabilities;
- The growth rate $\propto$ MRI amplitude;
- They may stop MRI growth;

Numerical Simulations of the MRI

- Numerical simulations show that the growth of the MRI mode is hampered by parasitic instabilities followed by transition to a turbulent state:

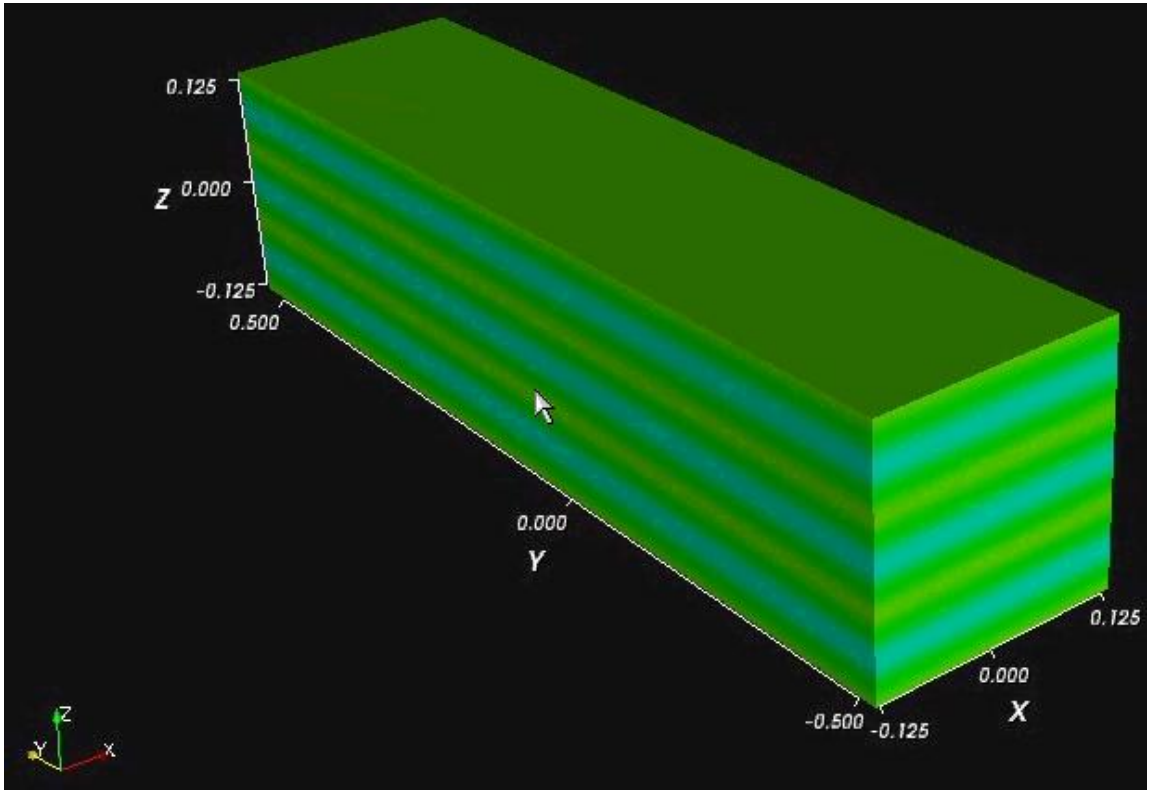

Numerical Simulations: Channel Solution

- Simulations show the formation of highly correlated states during which AM transport is very efficient.
- "Channel solutions" characterized by
  - peaks of Maxwell stress $\langle w_{xy} \rangle = \langle B_x B_y \rangle$
  - intermittent behavior
  - high correlation between magnetic field and velocity perturbations.
- Between adjacent peaks the system is turbulent and chaotic.
- Channel solution disrupted by secondary parasitic instabilities.

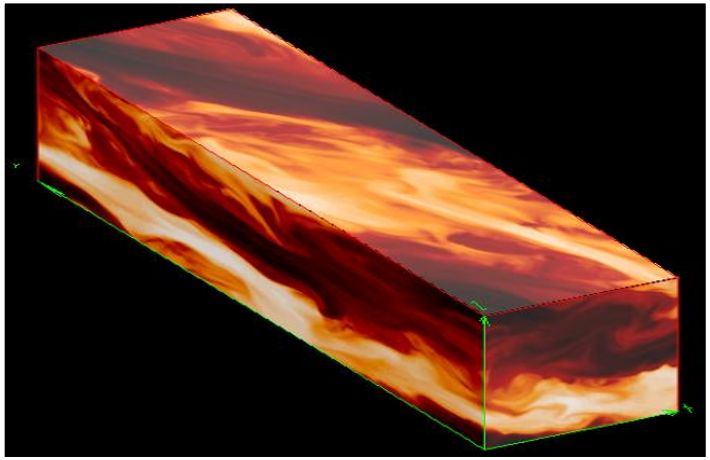

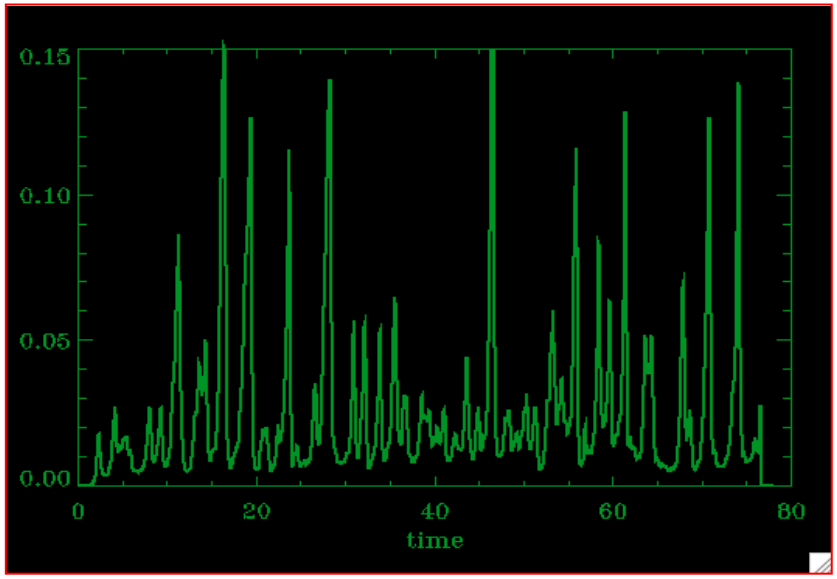

[1]Bodo et al., A&A(2008), 487,1B

Bx - By Correlation

- For a pure channel solution, B_x and B_y lie on a straight line with slope tan γ.
- In general we obtain scatter plots of magnetic field and velocity

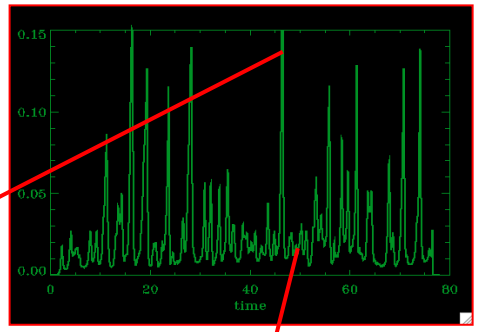

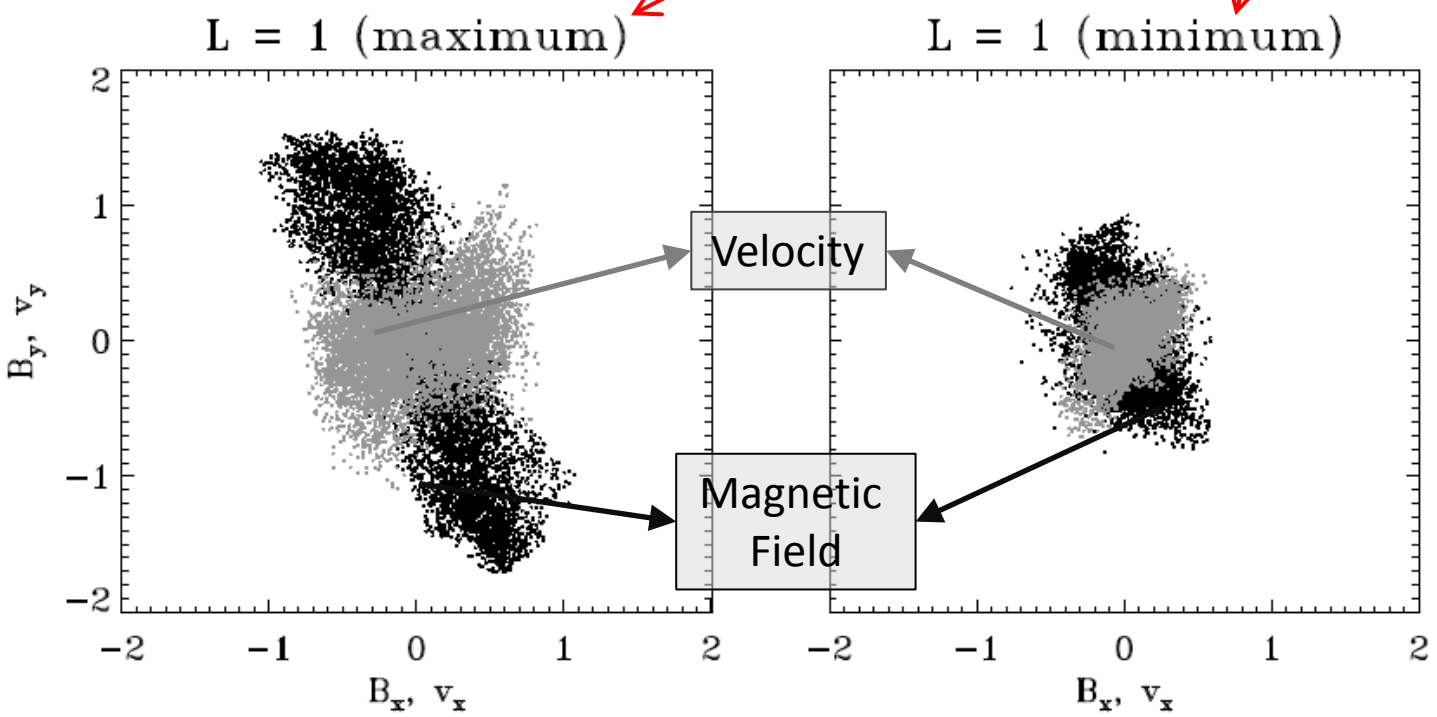

Aspect Ratio Dependence

- Numerical simulations of SB with different sizes (aspect ratio) $L \times 4 \times 1$ with L = 1, 4 and 8 reveal different behaviors[1] :

Maxwell Stresses

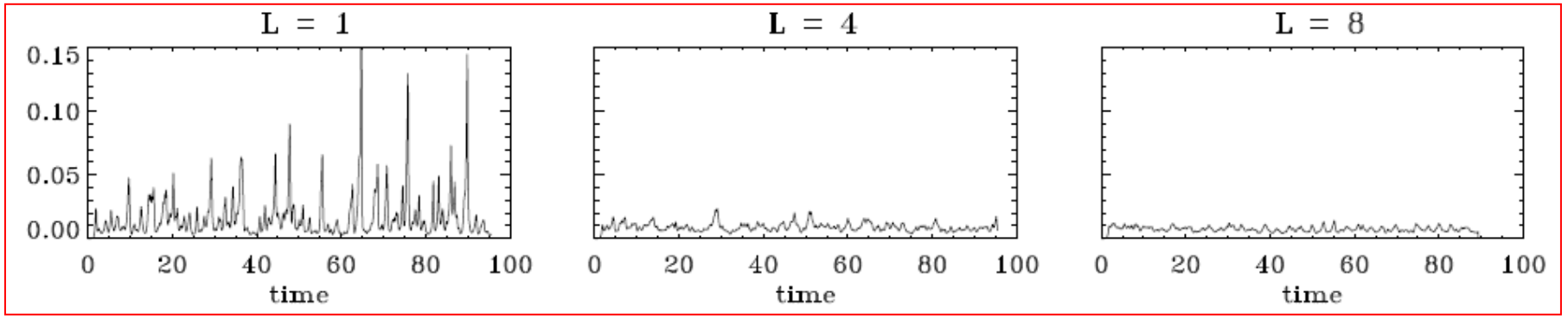

- $L \approx 1$ → solution features the channel solutions with high AM transport;
- Increasing the aspect ratio L, the channel solutions and the associated intermittent behavior disappear.

[1]Bodo et al., A&A(2008), 487,1B

Aspect Ratio: Distribution Between Peaks

Max

Min

L=1

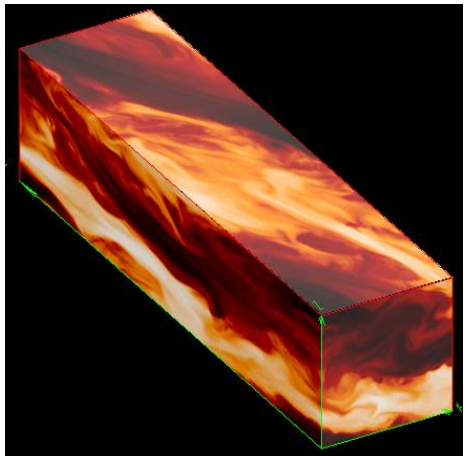

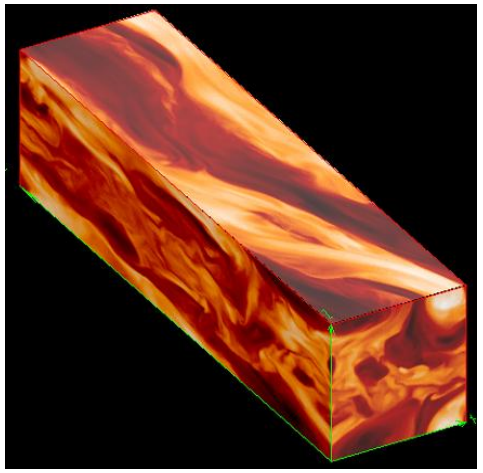

L=4

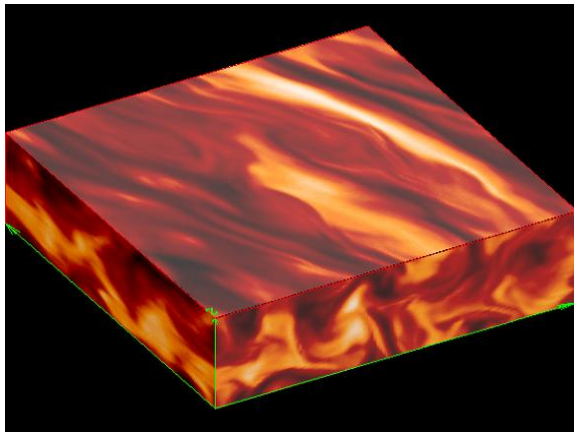

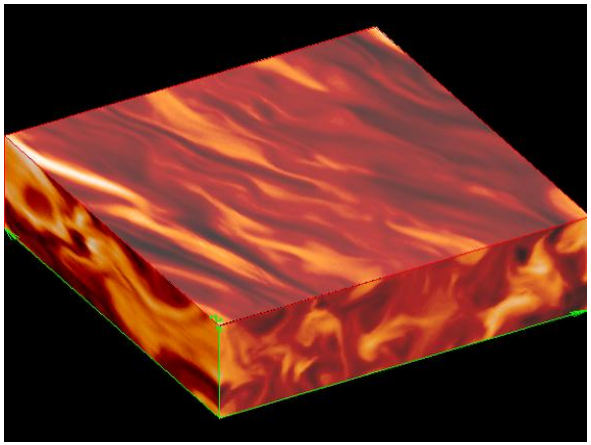

Aspect Ratio Dependence

- Dominance of the channel seems peculiarity induced by an overly constrained geometry[1];
- Possible explanation: parasitic instabilities have wavelength larger than vertical size of channel solution[2]. In box with L=1 they may simply be stable;
- In any case, it is clear that boxes with aspect ratios close to unity over-emphasize the role of the channel solutions and may lead to misleading results thus posing severe restrictions for applicability to real astrophysical systems.

[1]Bodo et al., A&A(2008), 487,1B; [2]Goodman, J., & Xu, G. 1994, ApJ, 432, 213

The Problem of Convergence: Zero vs Net Flux

- MRI-driven turbulence is studied in 2 different configurations: one with a *net magnetic flux (a)* threading the layer and the other in which there is *none (b)*.

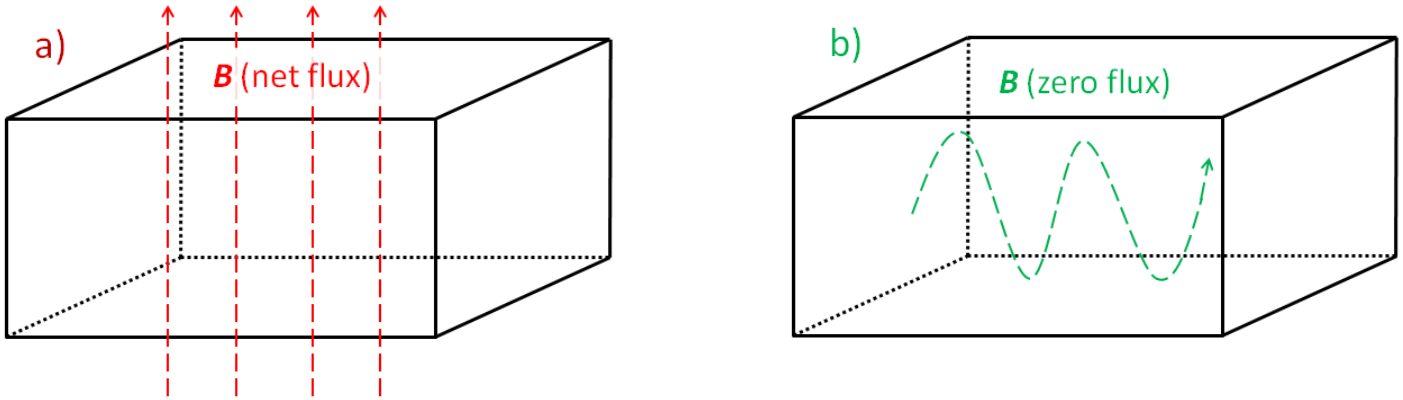

- In case *a)* there is a linearly unstable mode with a well defined vertical wavenumber of maximum growth rate that sets the scale of the instability;
- In case *b)* no such state exists, and the MRI must set in as a subcritical instability. The characteristic scale of the turbulence in the no net-flux case is, at present, an open question.

[1]Bodo et al., ApJ (2011) 739, 82

The Problem of Convergence for Zero Flux

- Conceptual appeal of the no-flux case: possibility of a universal state of MRI turbulence in which the disk becomes self-magnetized through dynamo action, and AM transport depends on the disk properties but not on the amount of flux threading the disk.

- Much effort has been devoted to determining if such a universal state exists, and the value of the associated turbulent transport.

- Simply stated, the problem of convergence is that AM transport measured in numerical simulations based on the SBA with zero mean flux depends on numerical resolution, and decreases as the resolution increases

The Problem of Convergence

- In the SBA with zero mean flux *the only intrinsic length is the* diffusive length scale ℓ_d.
- The size of the computational box *L* has no direct physical meaning.
- From this perspective, increasing the resolution and increasing the domain size are entirely equivalent operation.
- In the ideal limit, one can demonstrate[1] that the Shakura-Sunyaev coefficient α must scale as

$$\alpha \equiv \frac{1}{c_s^2}\overline{\left\langle u_x u_y - \frac{B_x B_y}{4\pi\rho} \right\rangle} \sim f_\delta(N)\frac{1}{N^2}$$

where N = number of grid points and $f_\delta(N)$ depends on the numerical scheme.

[1]Bodo et al., ApJ (2011), 739, 82

The Problem of Convergence: Results

- $\alpha \sim f_\delta(N)/N^2$ → in order for α to be resolution independent $f_\delta(N)$ must diverge as N^2.
- However: 5th-order accurate calculations show that the solution become asymptotically independent of the resolution

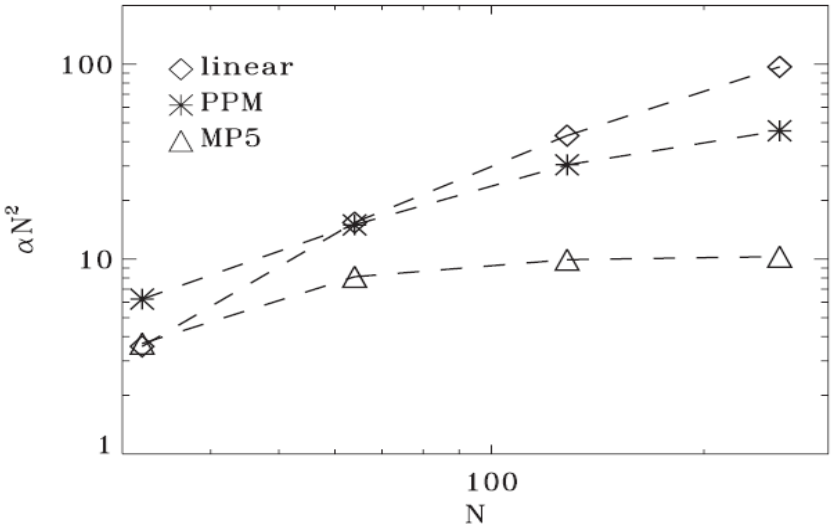

$$\alpha \sim f_\delta(N)\frac{1}{N^2}$$

- AM transport proportional to the diffusive flux and therefore has limited relevance in astrophysical situations.

[1]Bodo et al., ApJ (2011), 739, 82

Stratified SBA with Thermal Diffusivity

- Turbulence in stratified SB with zero mean flux reaches a stationary state in which thermal losses out of the boundaries are balanced by dissipative heating.

- Two regimes are identified:
  - Large κ → conductive regime in which the heat is transported mostly by conduction and the density decreases with height (~isothermal);
  - Small κ → convective regime in which the layer becomes unstable to overturning motions, the heat is carried mostly by advection, and the density becomes nearly constant throughout the layer.

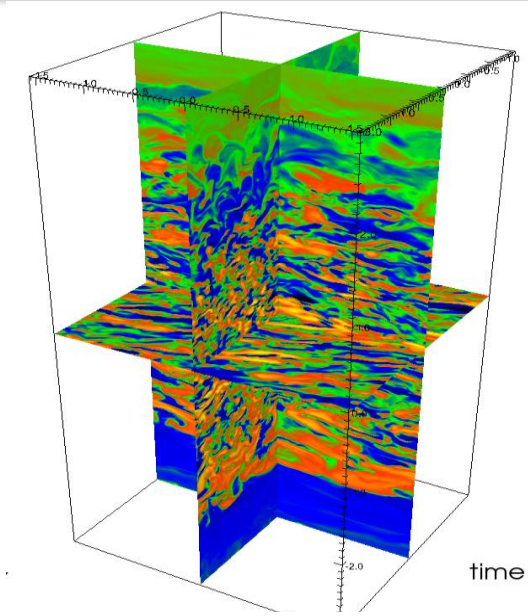

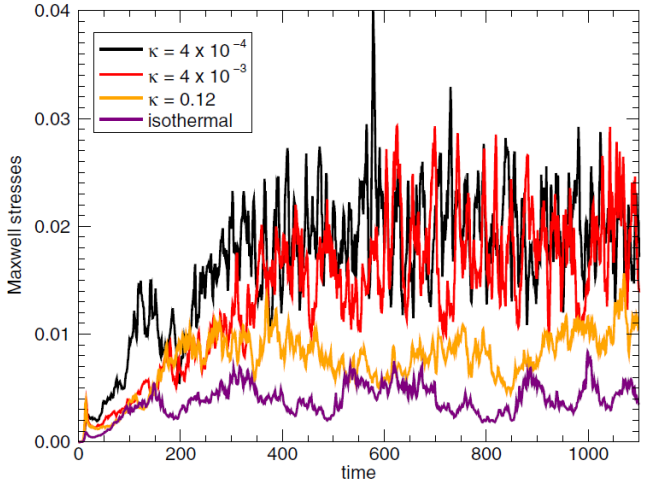

[1]Bodo et al., ApJ (2012), 761, 116

PART #4:
Global Models of Accretion Disks

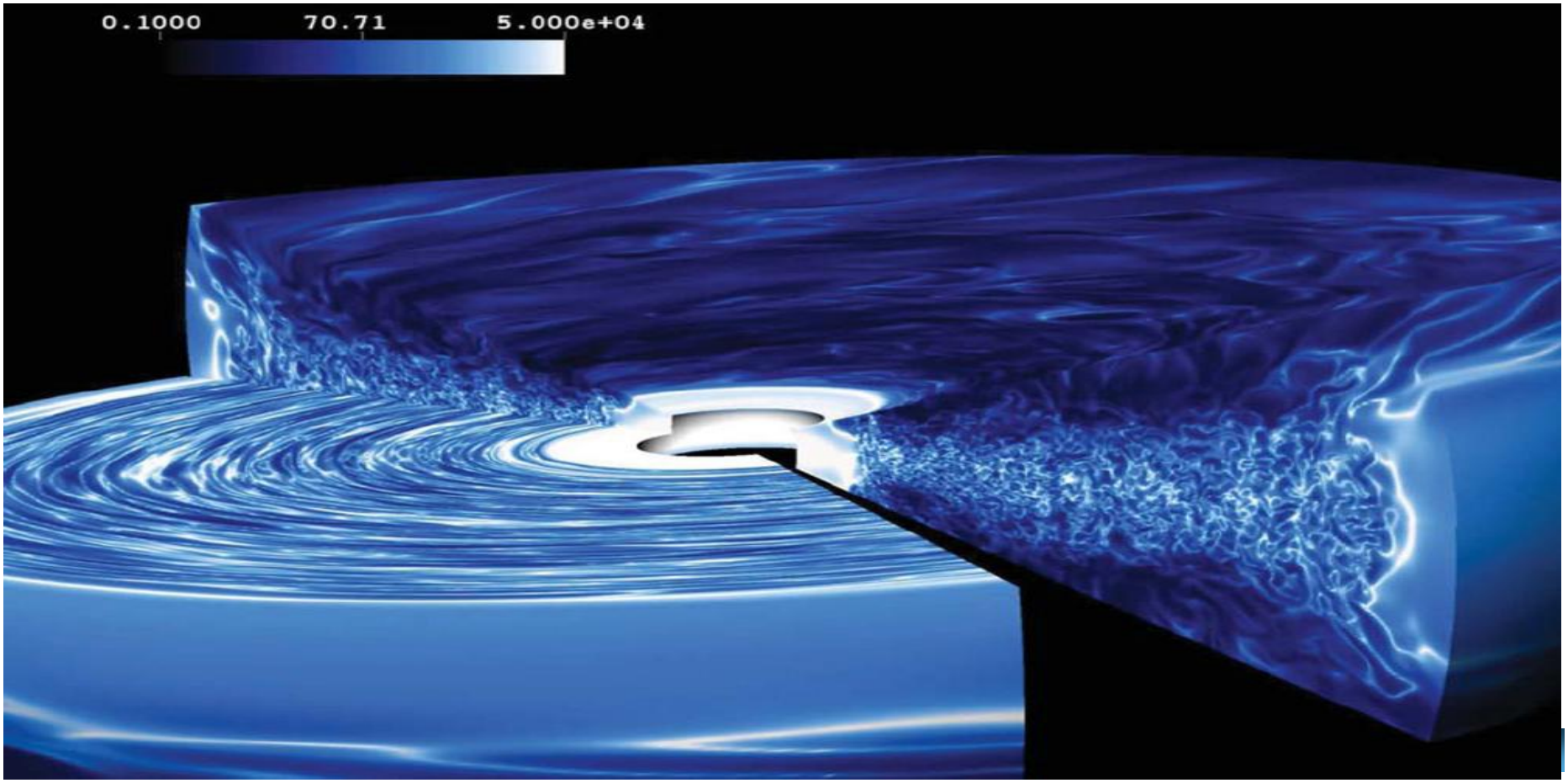

Toward Global Simulations of Accretion Disks

- Shearing-box approximation probably unable to capture the physics of MRI in disks.

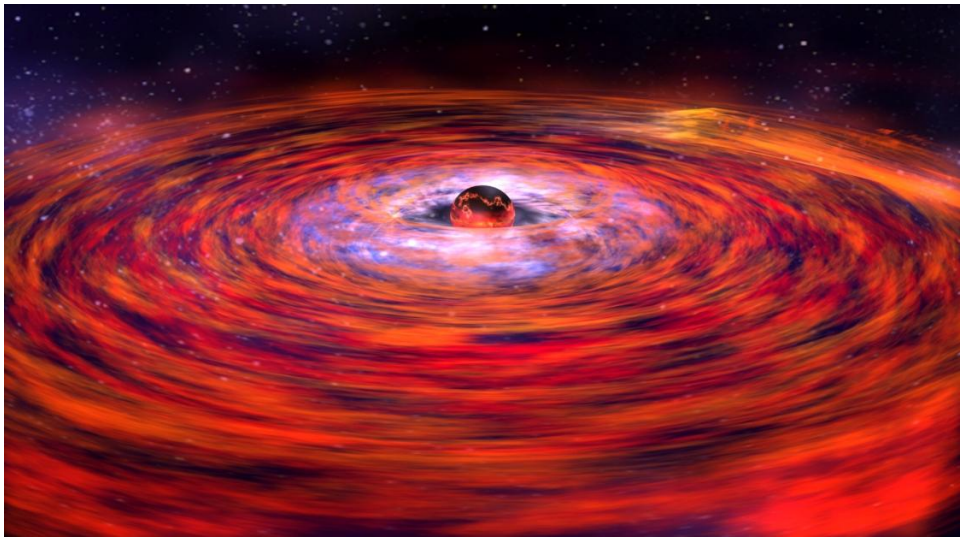

- Next generation simulations have to address the full disk problem;

- Challenge: the scale disparity from global disk to the turbulent dissipative scale is enormous and inaccessible to computation;

- Still: computations with sufficient scale separation may give important answers → need for very high resolution (> 10^9 points, disk storage> 200 TB).

Accretion Disks: axisymmetric models

- To reduce computational cost, previous models adopted considerable simplifications, e.g., axisymmetry;
- Limited applicability → need for 3D

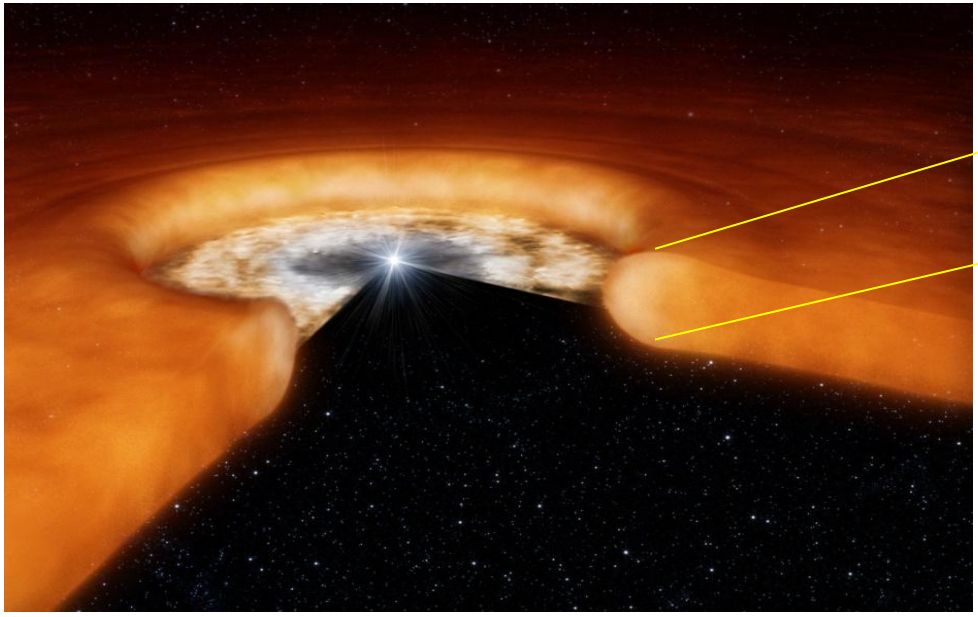

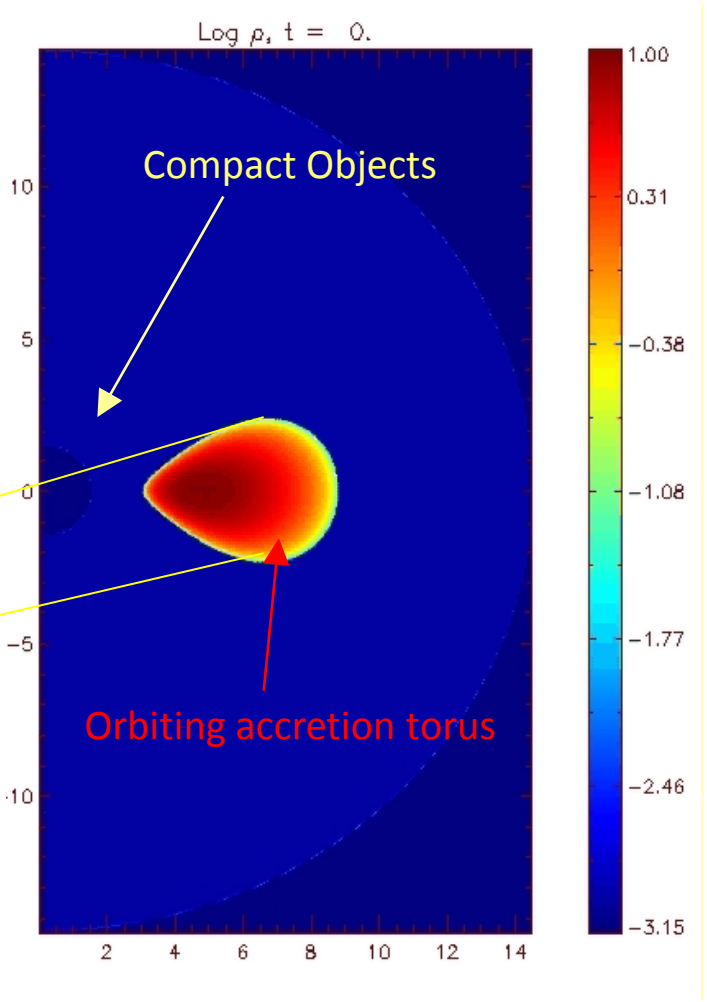

Global Models: Time Step Limitations

- Explicit computations of super-fast differentially rotating disks are subject to the CFL condition, $\Delta t \sim C_a \Delta l / \lambda_{max}$;
- In polar geometry $\Delta l \sim R\Delta\phi$ can diverge considerably across computational domain:

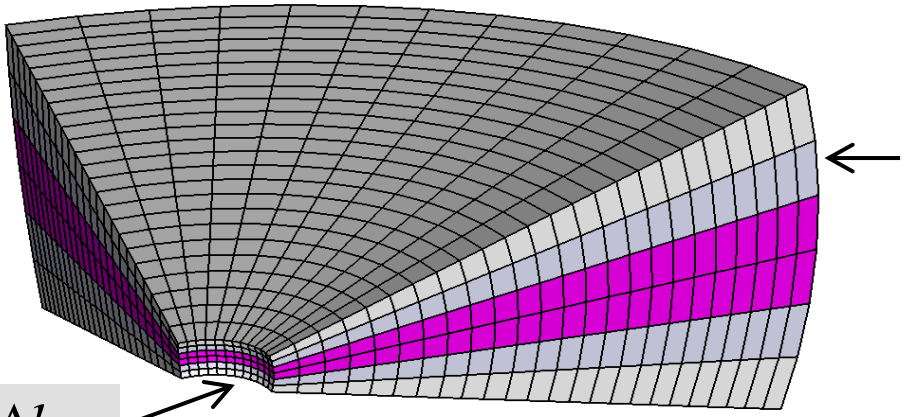

$$\Delta l_{min} \ll \Delta l_{max}$$

- Additionally, for super-fast magnetosonic flows,

  $\lambda_{max} = |V_k| + c_{fast} \gg c_{fast}$ and $V_k \sim R^{-3/2}$.

- Time step Δt severely limited by the inner zones !!

Overcoming the time step limitation…

- If velocity fluctuations are small, one may decompose $u = u' + u_0$, where u_0 = constant.
- An example: consider Burger's equation $$\frac{\partial u}{\partial t} + \frac{\partial}{\partial x}\left(\frac{u^2}{2}\right) = 0$$
- Decompose $u = u' + u_0$, so that $$\frac{\partial (u' + u_0)}{\partial t} + \frac{\partial}{\partial x}\left[\frac{1}{2}(u' + u_0)^2\right] = 0$$
- Doing the math: $$\frac{\partial u'}{\partial t} + \frac{\partial}{\partial x}\left[\frac{(u')^2}{2}\right] + u_0\frac{\partial u'}{\partial x} = 0$$
- Thus one can solve Burger's equation in the residual u' and then "shift" the equation with constant speed u_0 :

$$u(x,t) = u'(x - u_0 t, t);$$

Orbital Advection: the FARGO Scheme

- By decomposing the total velocity into an average azimuthal contribution and a residual term, the MHD equations can be solved through two separate steps corresponding to:

    1. a linear transport operator in the direction of orbital motion and
    2. a standard nonlinear solver applied to the MHD equations written in terms of the residual velocity.

- Since step 1) is not subject to any stability restriction, the CFL condition depends on the residual velocity, leading to substantially larger time steps.
- This is called the FARGO (***F**ast **A**dvection in **R**otating **G**aseous **O**bjects*)[1,2] scheme.

[1]Masset, A&A (2000) 141,165; [2]Mignone et al., A&A (2012) 545, A152

The FARGO-MHD Equations

- With the decomposition $\boldsymbol{v} = \boldsymbol{v}' + \boldsymbol{w}$ one obtains[1] the following

$$
\begin{aligned}
\frac{\partial \rho}{\partial t} + \nabla \cdot (\rho \boldsymbol{v}') + \boldsymbol{w} \cdot \nabla \rho &= 0 \\
\frac{\partial (\rho \boldsymbol{v}')}{\partial t} + \nabla \cdot (\rho \boldsymbol{v}' \boldsymbol{v}' - \boldsymbol{B}\boldsymbol{B} + \mathsf{I} p_t) + \boldsymbol{w} \cdot \nabla (\rho \boldsymbol{v}') &= \boldsymbol{S}'_m - \rho \nabla \Phi \\
\frac{\partial E'}{\partial t} + \nabla \cdot \left[(E' + p_t) \boldsymbol{v}' - (\boldsymbol{v}' \cdot \boldsymbol{B}) \boldsymbol{B} \right] + \boldsymbol{w} \cdot \nabla E' &= S'_E - \rho \boldsymbol{v}' \cdot \nabla \Phi \\
\frac{\partial \boldsymbol{B}}{\partial t} - \nabla \times (\boldsymbol{v}' \times \boldsymbol{B}) - \nabla \times (\boldsymbol{w} \times \boldsymbol{B}) &= 0
\end{aligned}
$$

- Use operator splitting to solve for
  - the nonlinear step: $\mathcal{L}_n(q)$: $\dfrac{\partial q}{\partial t} + \nabla \cdot \boldsymbol{F}_q = S_q$
  - the linear transport step: $\mathcal{L}_t(q)$: $\dfrac{\partial q}{\partial t} + \boldsymbol{w} \cdot \nabla q = 0.$

[1] Mignone et al., A&A (2012) 545, A152

Example: Disk-Planet Interaction

- Problem: Jupiter-mass planet embedded in a viscous global disk.
- Domain: 3D spherical coordinates, with (N_r, N_θ, N_ϕ = 256, 32, 768).
- Speedup ~ 4

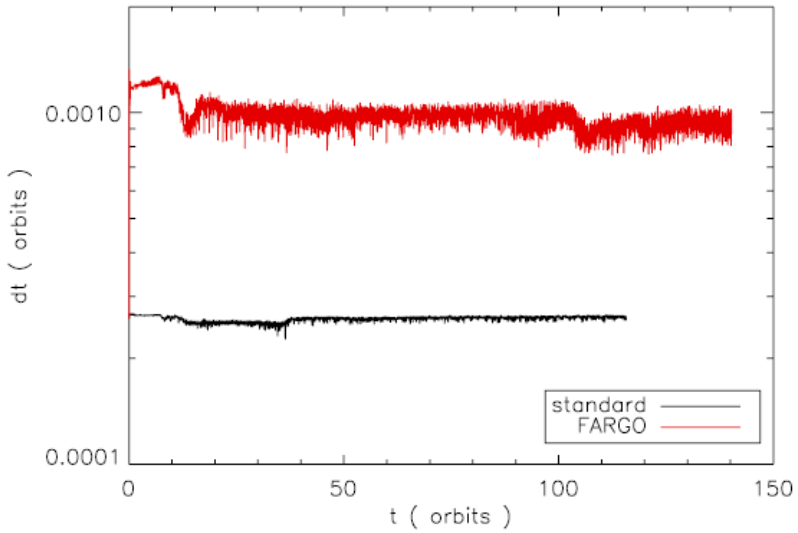

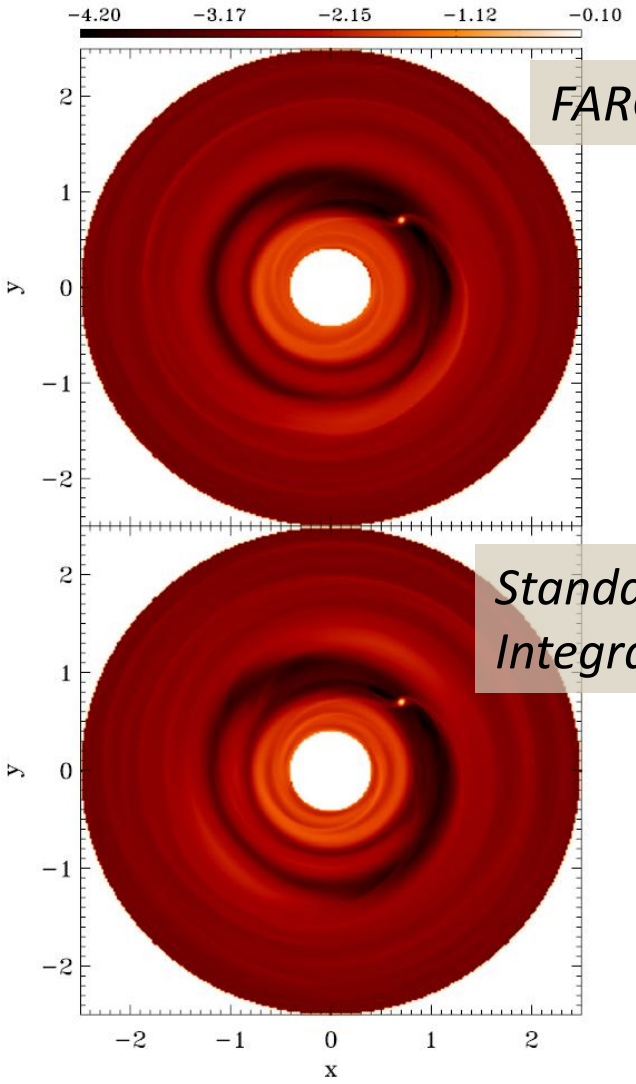

Example: MRI

- Problem: global disk simulation;
- Domain: spherical coordinates r, θ, ϕ, resolution 384 x 192 x768
- Orbital advection gives a speedup ~ 4
- Reduced numerical dissipation → larger α

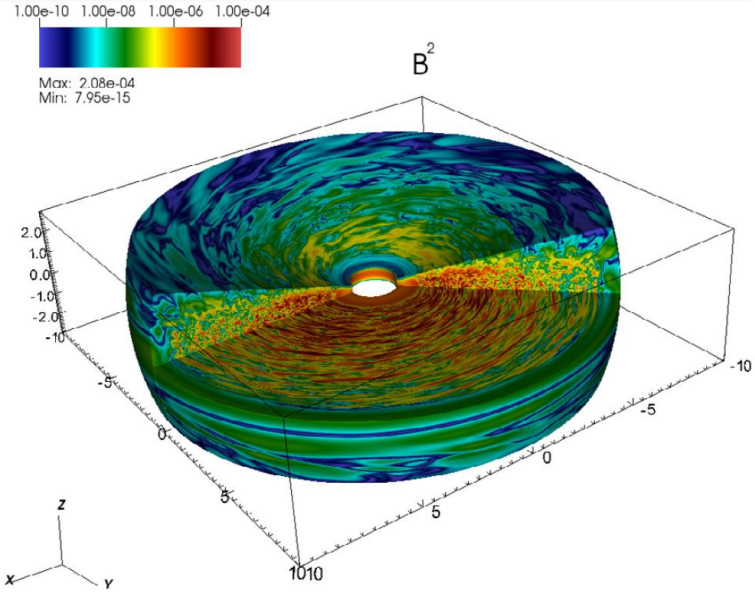

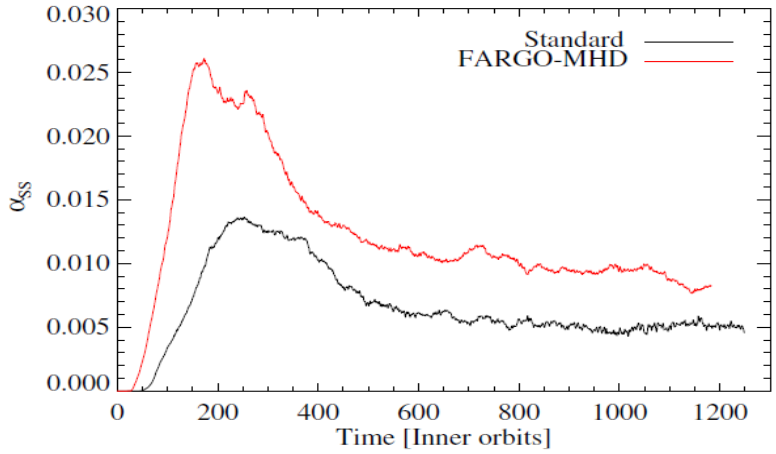

3D Simulations of Stratified Magnetized Disks

- Fully 3D, simulation of stratified global disk by Flock et al[1] using the PLUTO code.
- Zero net flux;
- Spherical coordinates r, θ, ϕ, resolution 384 x 192 x768
- +- 4.3 vertical scale heights; $0 < \phi < 2\pi$
- ~10 TB of data

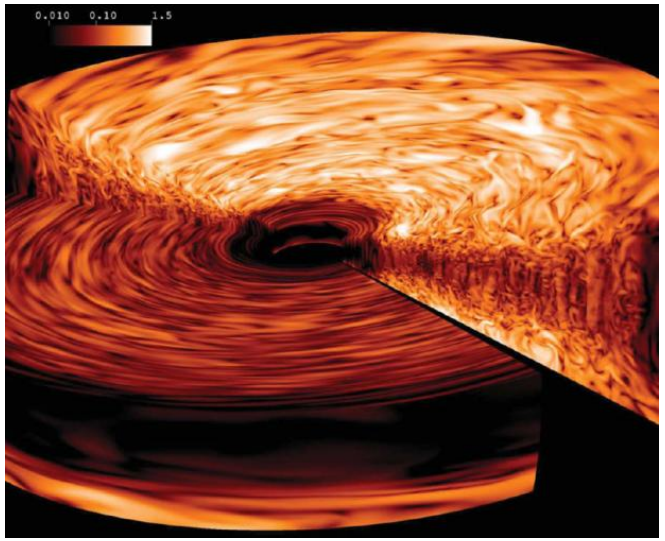

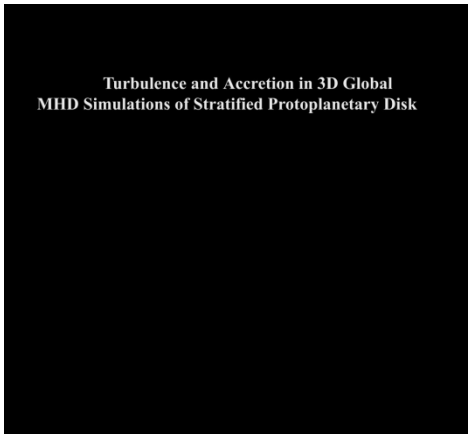

[1]Flock et al., A&A (2012) 735, 122

3D Simulations of Stratified Magnetized Disks[1]

- Need > 25 zones per pressure scale height;
- $\alpha \sim$ 5.e-3
- Steady state turbulence after ~250 inner orbits and before 1200
- Results compatible with local box simulations.
- Energy spectra peaks for m=3 and m=5
- No evidence for Kolmogorov-type scaling

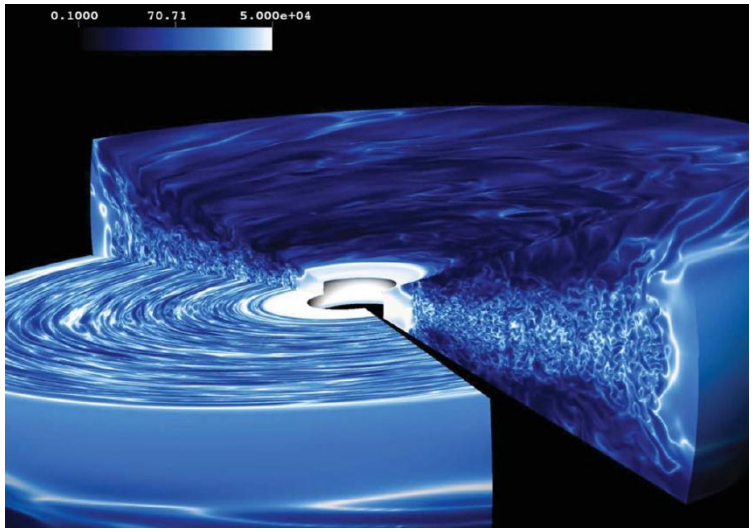

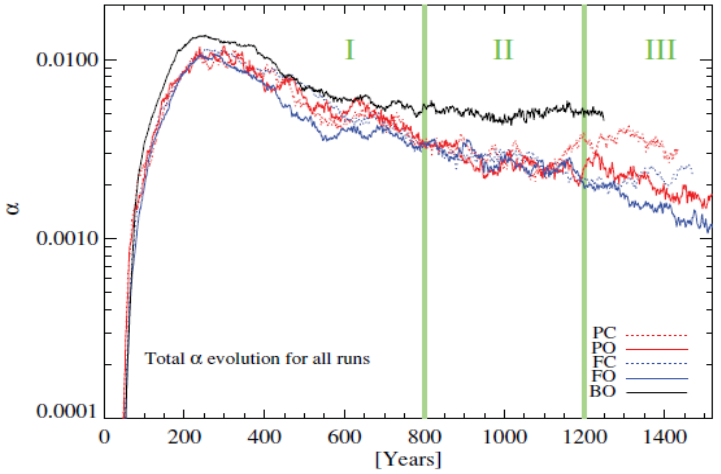

[1]Flock et al., A&A (2012) 735, 122

Other Results…

- Beckwith et al, MNRAS (2011):
  - Use pseudo-Newtonian potential
  - α = 2.5e-2
- Sorathia et al. (2012)
  - Convergence and comparison with local models;
- Flock et al, ApJ (2012):
  - Large scale azimuthal magnetic structures of turbulence;
  - Stronger turbulence state in restricted azimuthal domain;
- Parkin Bicknell, ApJ (2013):
  - Test the linear growth of MRI starting from equilibrium models;
  - Saturated state independent of the initial MRI mode

PART #5:
Magnetically Driven Outflows

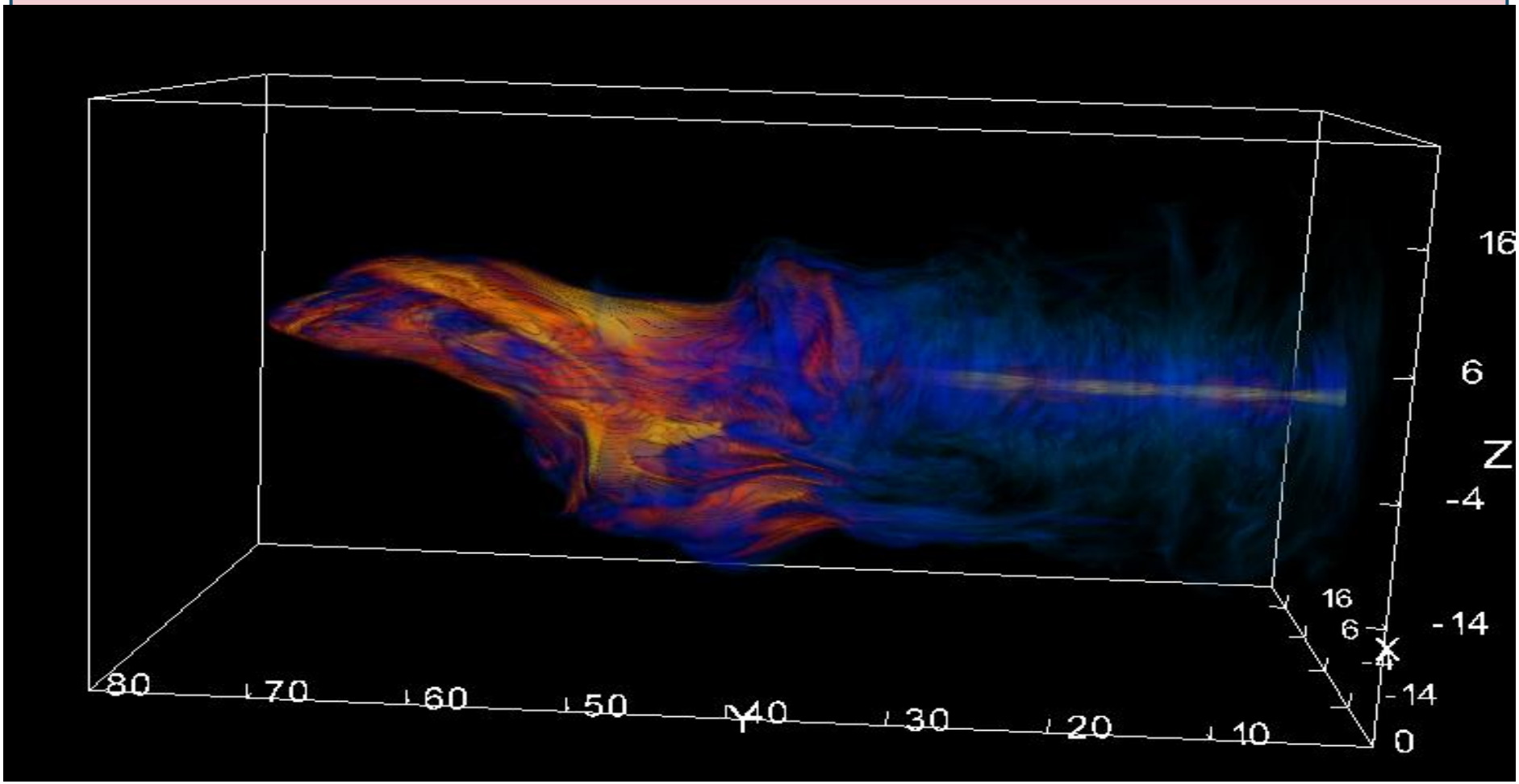

Magnetically Driven Outflows

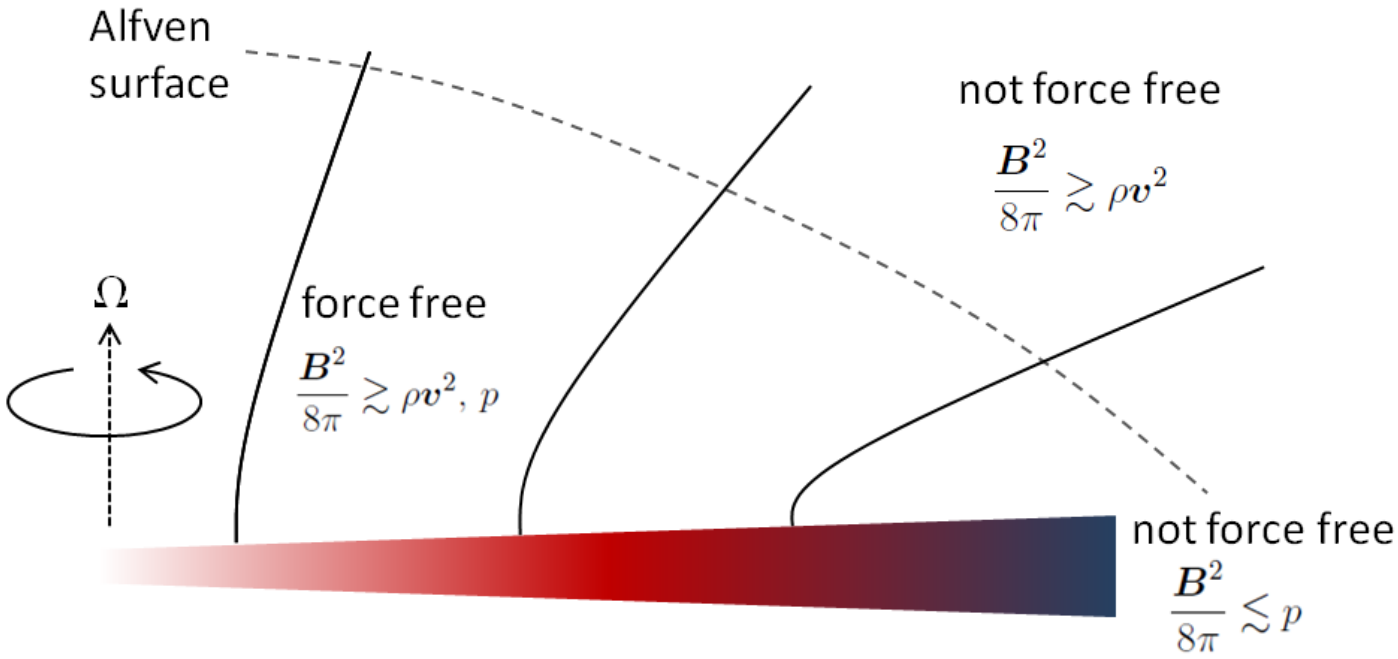

- Keplerian disk threaded by a poloidal field anchored to it.
- At the footpoint, gravity is balanced by the centrifugal forces;
- Above the disk a hot under-dense corona corotates with the disk;

Magnetically Driven Outflows

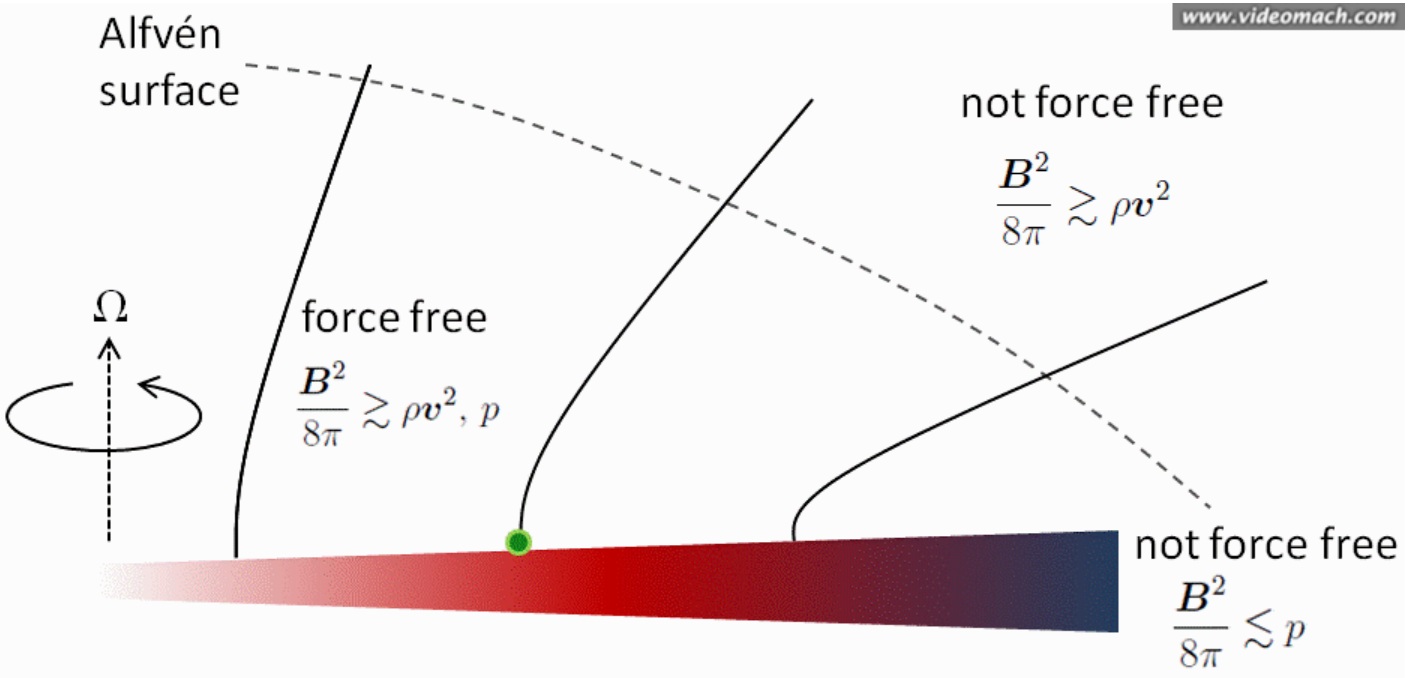

- Lorentz force ⊥ to the field: gas free to move along field files under the action of other forces like a 'bead on a wire'.
- When $\Omega^2 R > GM/R^2$ the gas element is accelerated outward.
- Acceleration stops at the Alfvén surface where the $V_{flow} > V_{Alfvén}$ and the field is no longer strong enough to enforce corotation.

Magnetically Driven Outflows

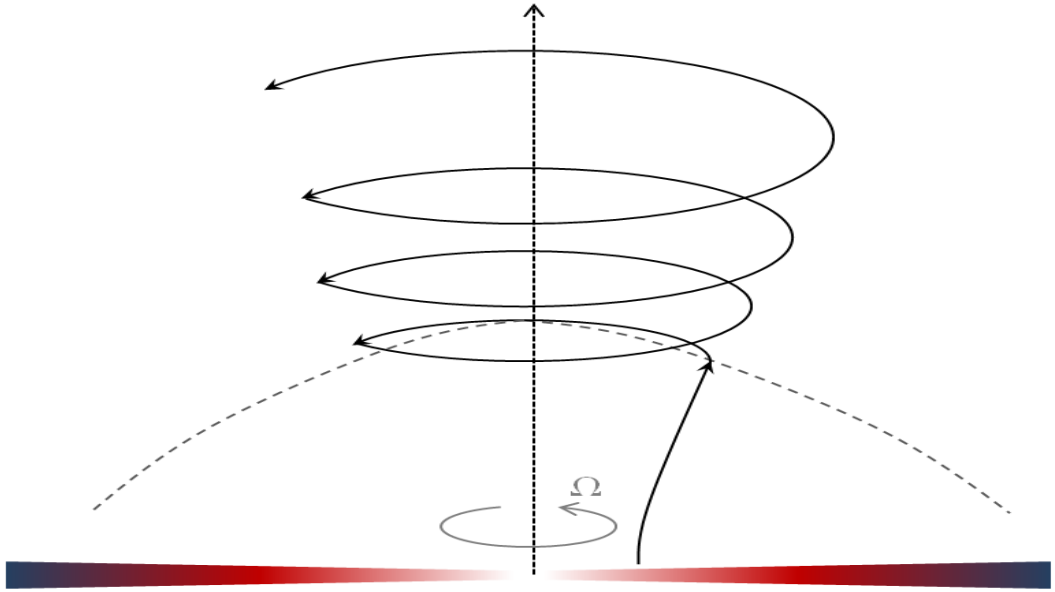

- Beyond the Alfvén surface, the inertia of the gas causes it to lag behind the rotation and the field winds up.
- Schematically, for each rotation of the foot point, one loop of the field is added at the surface.
- As the flow carries loops away, a spiral-shaped magnetic field forms;

Magnetically Driven Outflows

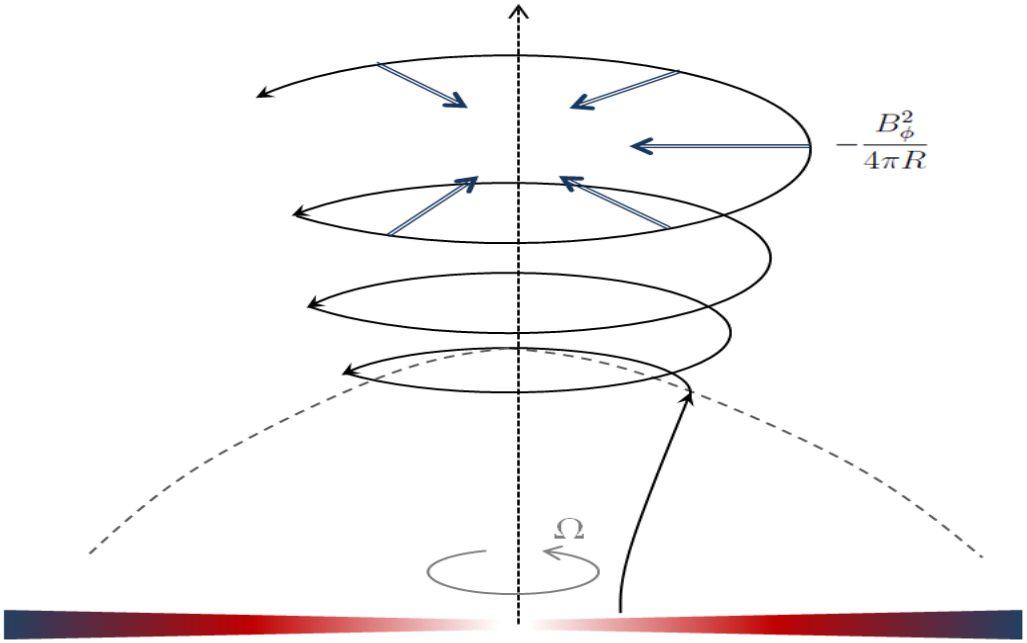

- Collimation phase: the curvature of the azimuthal field is directed towards the axis causing the flow to 'collimate' becoming parralel to the rotation axis → "*Hoop Stress*".
- The wind and the jet carry both kinetic and magnetic energy;
- Close to the disk, MHD Poynting flux leaves the disk.

Magnetocentrifugal Mechanism: Simulations

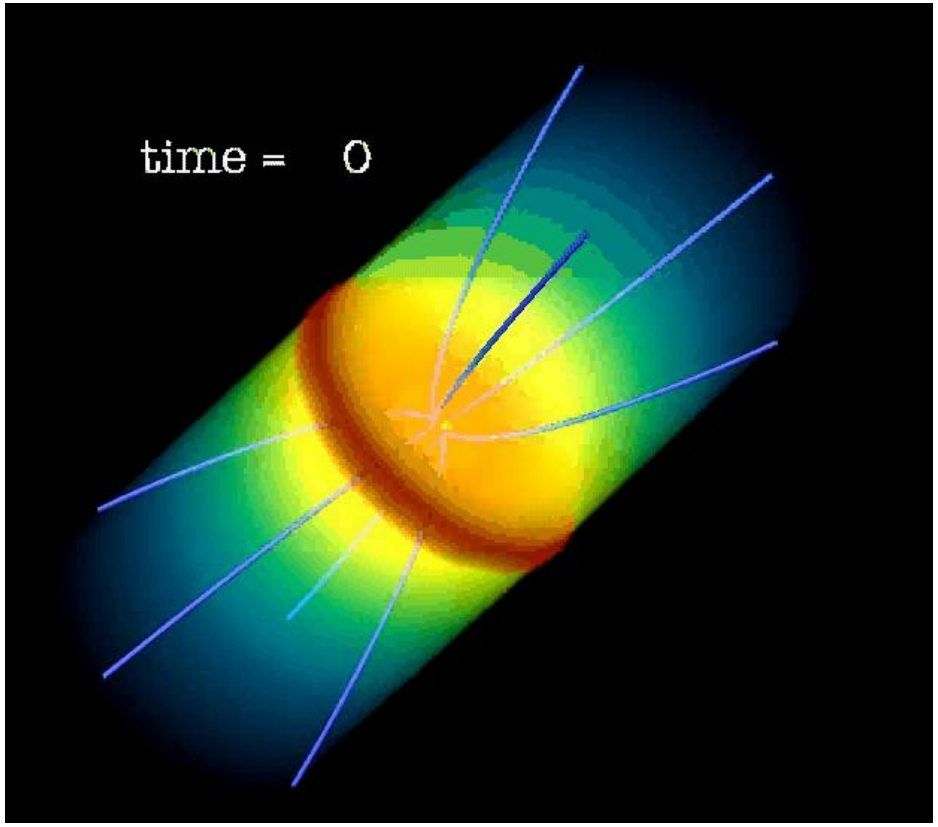

Zanni et al., A&A (2007) 469, 811

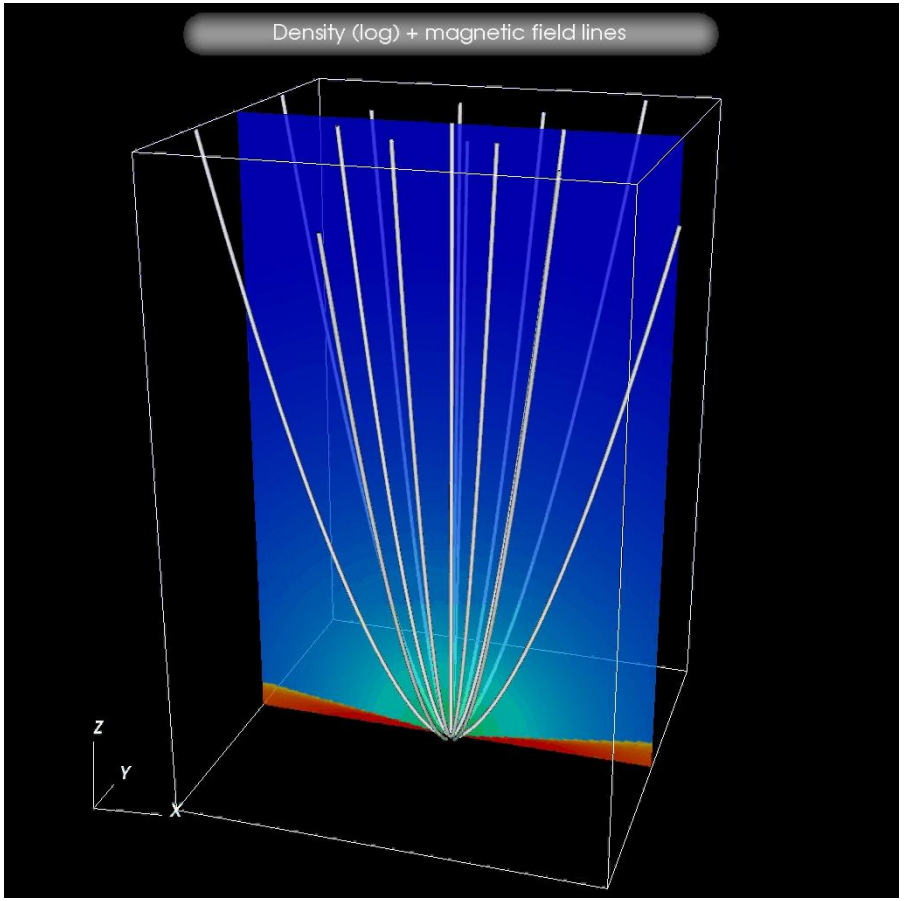

Tzeferacos et al., MNRAS (2009) 400, 820

Next Computational Challenges

- Future computations should be link jet launching process with fully 3D accretion disk models (first attempts underway[1])

- Large distance propagation may answer several questions:
  - how do jet survive to instabilities ?
  - where does the poynting / matter dominated transition occurs ?
  - how does the jet brake (FRI / FRII dicothomy) ?

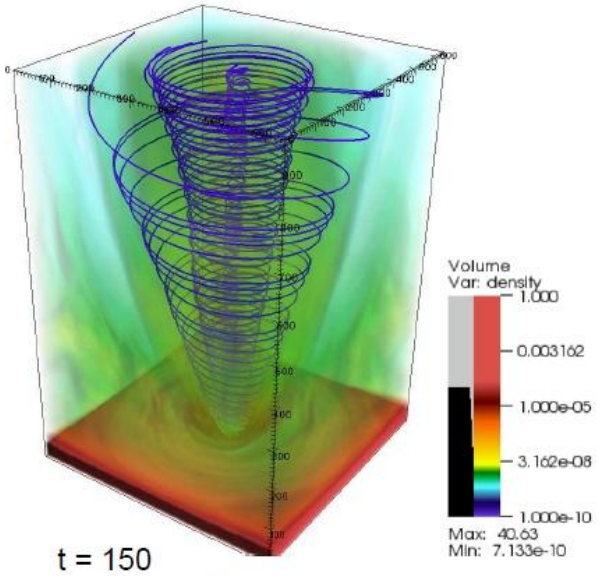

- Non ideal effects (resistive MHD, radiation transport and non thermal emission processes) likely to extend our current view.

[1]Zanni et al, submitted

PART #6
Jet Morphology & Propagation

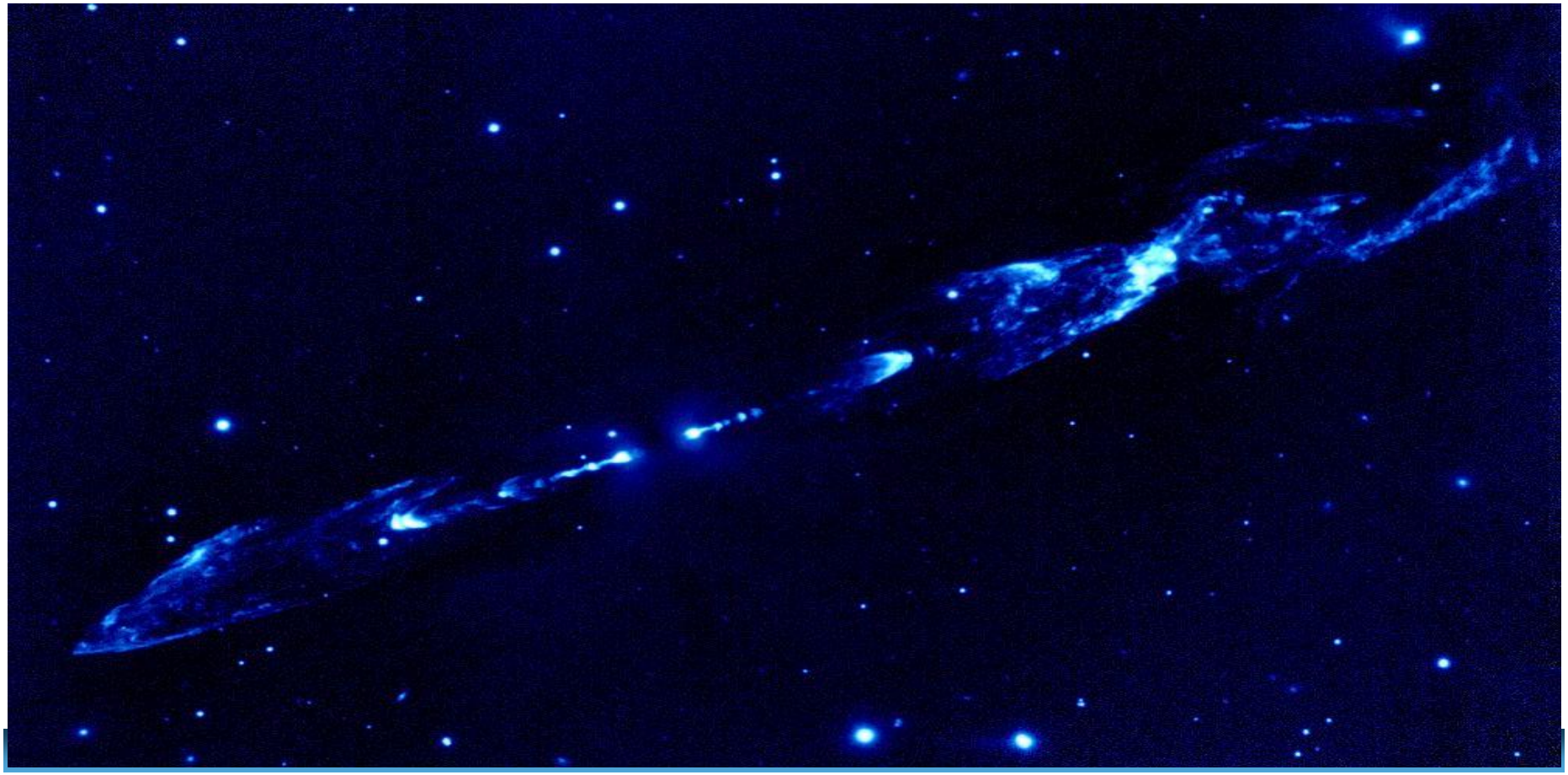

Stellar Jets from Young Stellar Objects

- Jets from star-forming regions generate strong shock waves that heat and ionize the gas.
- Main cooling source: collisional excitation of low-lying energy levels → emission line spectrum;
- Forbidden emission lines in the optical, IR;
- *Challenge*: emitting radiation from localized thin post-shock regions → resolve different time and spatial scales:
  - Advection scales ~ 10 yrs/ ~10^{15} cm
  - Cooling scales ~ week / ~10^{13}-10^{12}cm (! Stiff !)

Physical Model

- MHD Jet models consider optically thin cooling + ionization network to reproduce the dynamics and emission properties of secondary shocks moving along the jet beam:

$$\frac{\partial E}{\partial t} + \nabla \cdot \left[(E + p_t)\, \boldsymbol{v} - (\boldsymbol{v} \cdot \boldsymbol{B})\, \boldsymbol{B} \right] = S_E$$

$$S_E = -\left(N_{\rm at} N_{\rm el} \Lambda\left(T, \boldsymbol{X}\right) + L_{\rm FF} + L_{\rm I-R} \right)$$

$$\frac{\partial (\rho X_{\kappa,i})}{\partial t} + \nabla \cdot (\rho X_{\kappa,i} \boldsymbol{v}) = \rho S_{\kappa,i}$$

- In PLUTO we employ a chemical ionization network with a Multi-Ion Non Equilibrium (MINEq) cooling function[1]:

  - HI, HII, HeI, HeII, C(I-V), N(I-V), O(I-V), Ne(I-V), S(I-V)
  - Collisional ionization
  - Radiative & Dieletronic recombination
  - Charge transfer, H <-> He

[1]Tesileanu et al., A&A (2008) 488, 429

One-dimensional calculations

- Emission comes from very localized regions behind the shock
- Need for adaptive mesh refinement following the shock[1]:

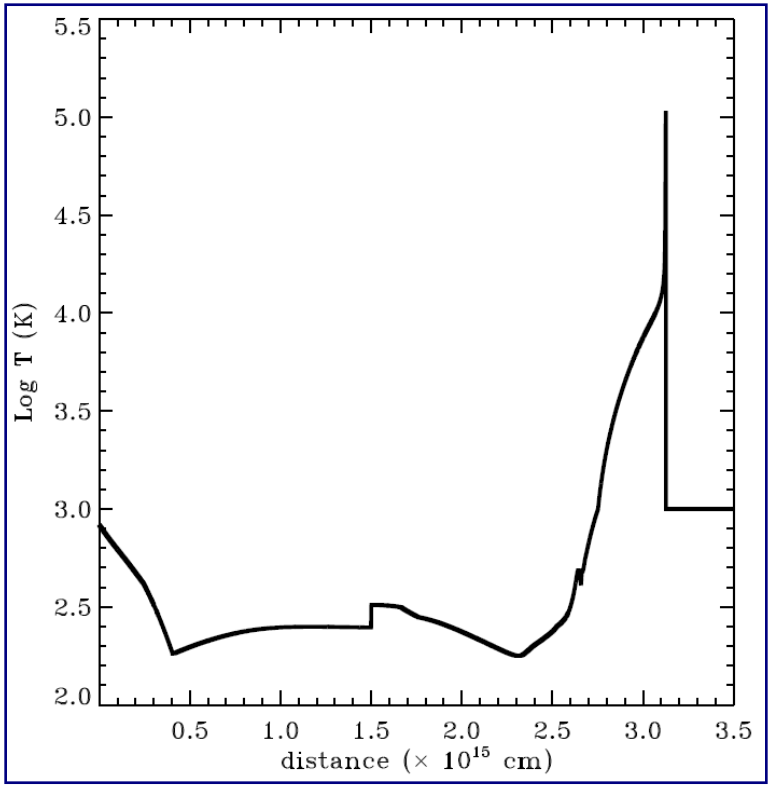

Static uniform grid (49152 zones), ~ 17 hrs

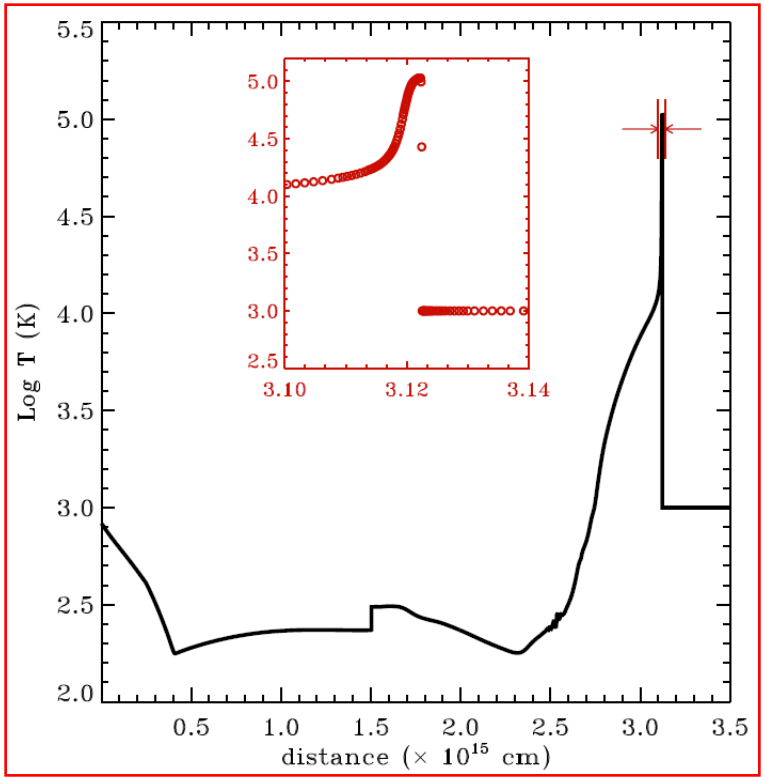

AMR (1536, 5 levels) ~ 4 min

[1]Tesileanu et al., ApJ (2012) 746:96

2D AMR Models Using PLUTO

Problem:

Radiative pulsed jet[1,2]

Base Grid:

128x640

Levels of Refinement:

7 (eq. Res = 16384x81920)

Method:

Unsplit PPM + Cooling

Code:

PLUTO + Chombo Lib

Description:

Jet perturbed at the inflow with a velocity variability (T = 50 yrs). Parameters:

$n_H = 500\ cm^{-3}$,

$v_j = 200$ Km/s

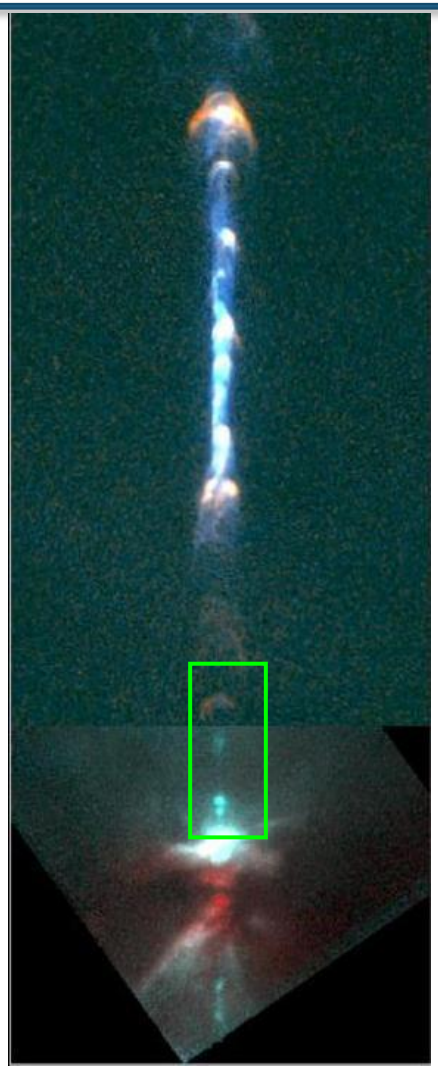

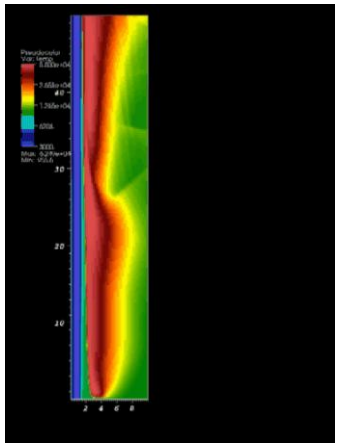

[1]Tesileanu et al., ApJ (2012) 746:96, [2]Tesileanu et al., A&A (2009) 507, 588

Comparison with Observations

- Different jet configurations are compared to observational data by constructing synthetic emission maps, spectra and P-V diagrams of single lines.

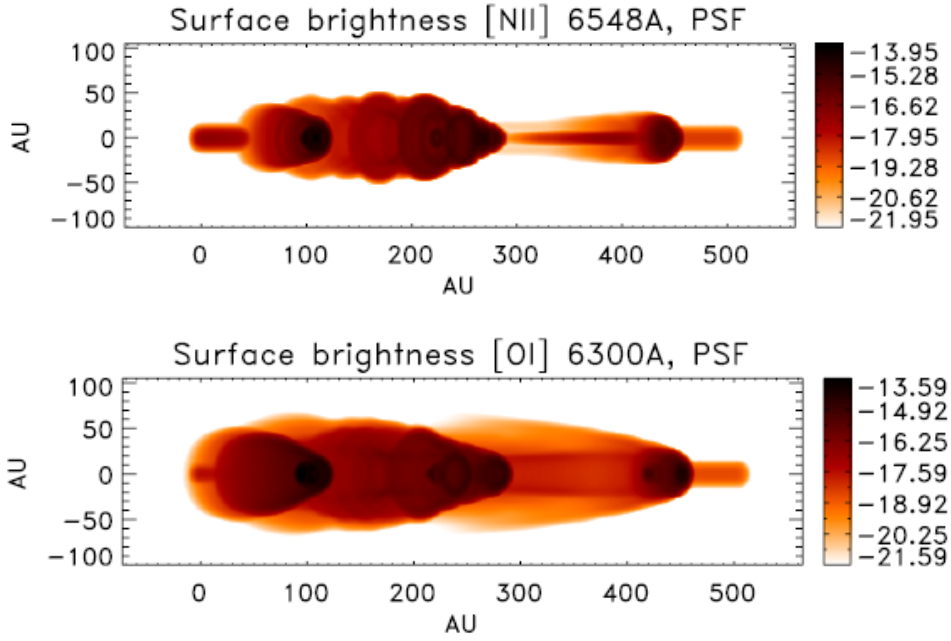

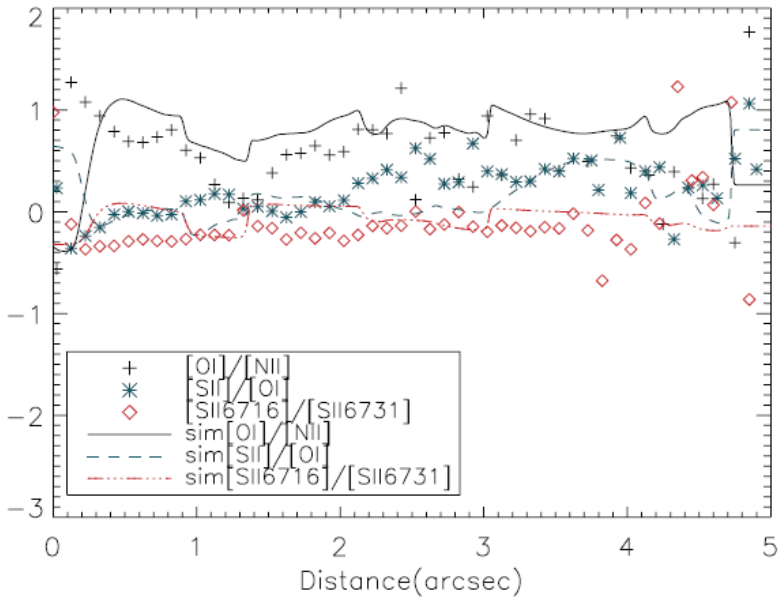

[1]Tesileanu et al., ApJ (2012) 746:96

Extragalactic Jets: Morphology

- Supersonic, highly collimated plasma ejecta propagating away from the central engine

- Fundamental questions:
  - how can jet survive fluid instabilities ? Confinement ?
  - Morphology ⇔ physical properties (density, composition, magnetic fields…) ?
  - Jet emission mechanism ?
  - how do they decelerate ?

- Understanding the processes leading to momentum, energy and mass transfer to the environment is crucial and still largely unanswered.

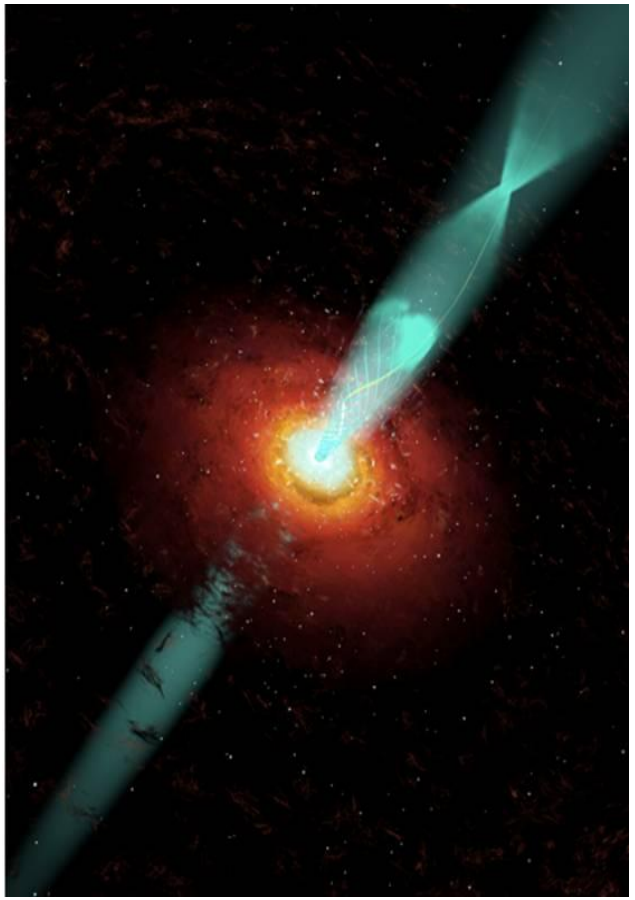

Fanaroff-Riley Morphological Classes

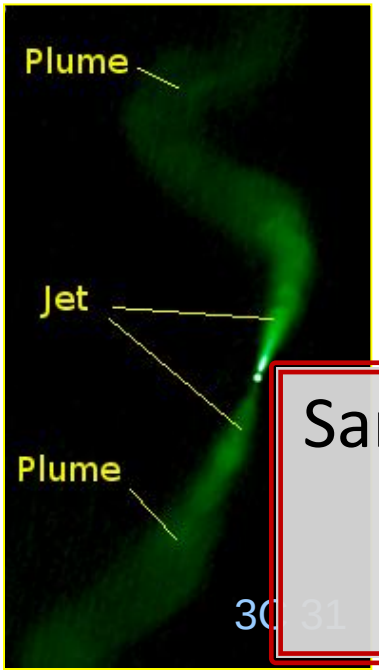

FR I

Low power sources, brightest towards the center, fainter at the end. Two-sided jets associated with bright large galaxies. Larger opening angles.

FR II:

High power sources, dominated by lobe emission (hot-spots), found isolated or in poor groups among emission lines galaxies. Smaller opening angles. "Knotty structure"

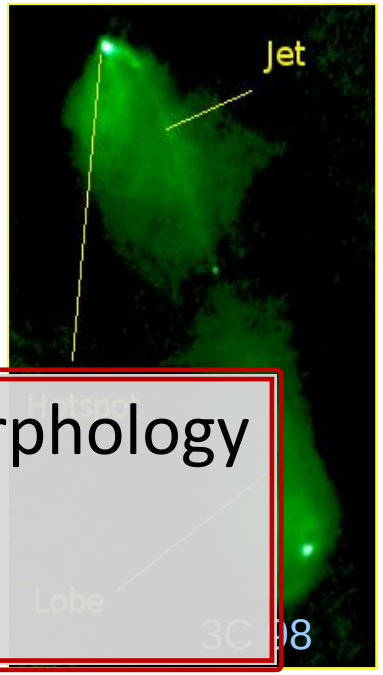

Same central engine but different morphology

Why ??

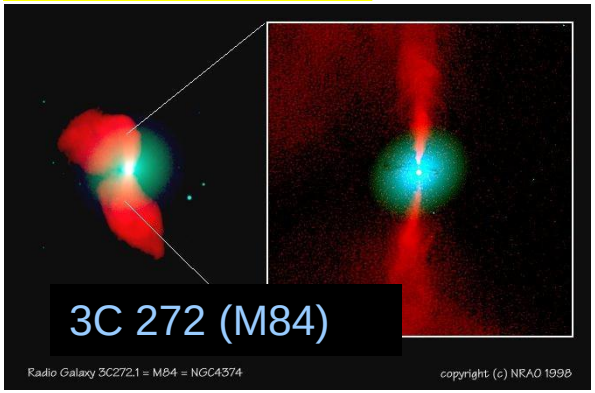

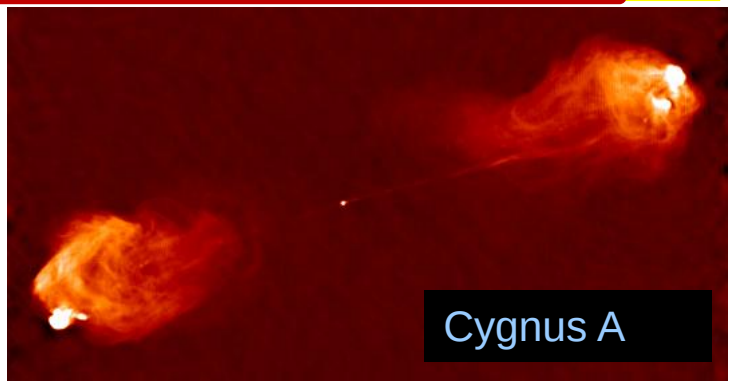

On the Jet Density: preliminary results

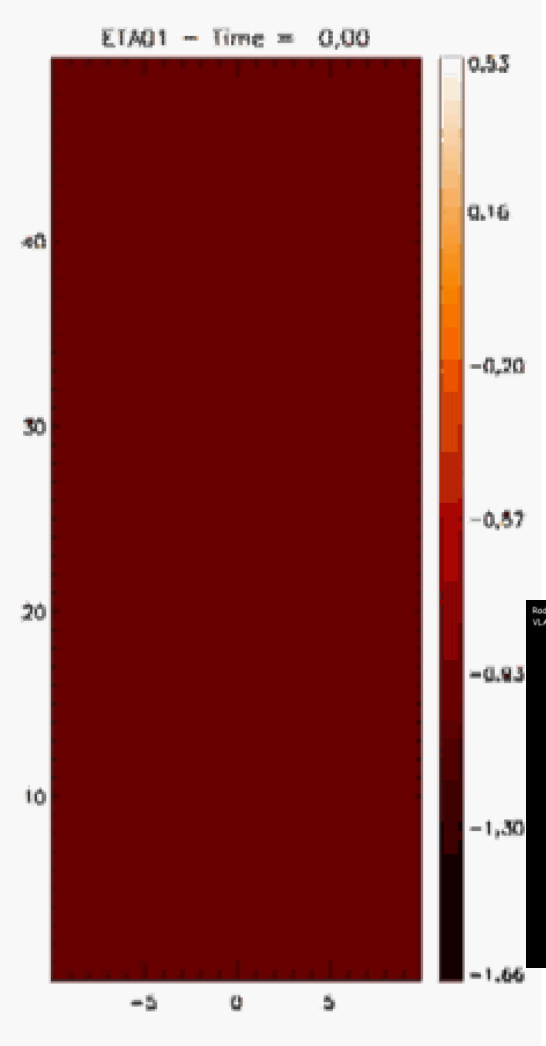

Prominent cocoon and backflows can be formed only for underdense jets:

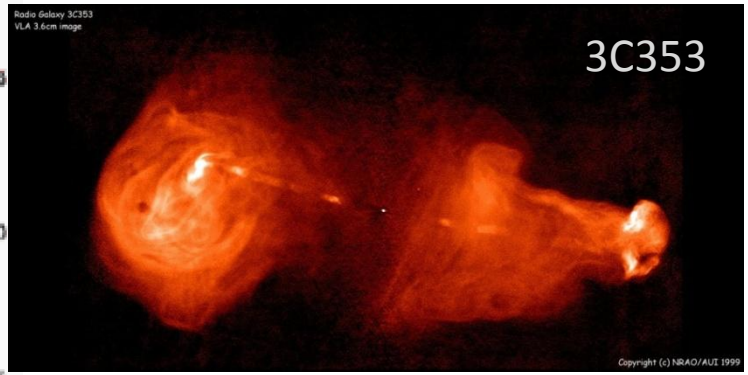

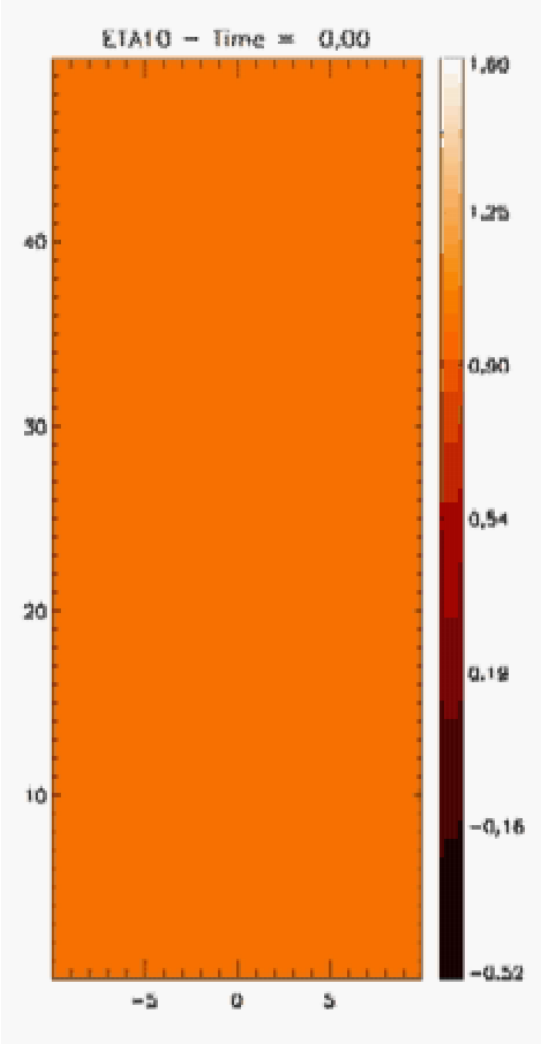

Fluid Instabilities In Jets

- Kelvin-Helmholtz Instabilities:
  - triggered by the presence of velocity shear
  - Act at the jet/ambient interface.
  - Induce mixing and momentum/energy transfer from jet to ambient

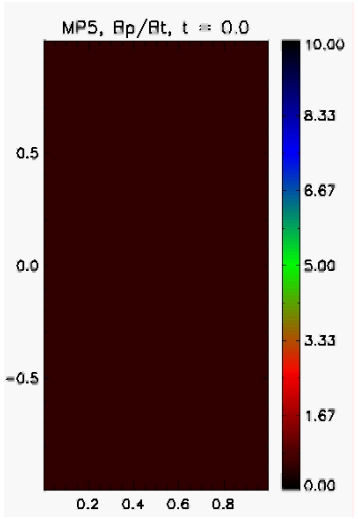

- Current-Driven Instabilities:
  - Triggered by the presence of a poloidal current;
  - induce large.scale jet deformation / compression

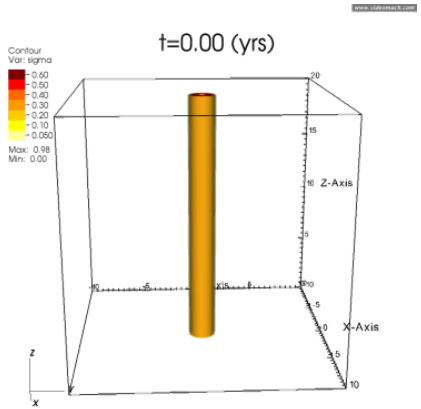

- Other kind of instabilities may be present (Pressure Driven, MRI, Firehose, etc…)

Onset of Current-Driven Instabilities in 3D

- Three-dimensional dynamics very different from 2D models.
- CD kink instabilities (|m|=1) can easily induce “kink” and large scale deflection of the jet creating multiple shock sites[1].

2D, axisymmetric propagation

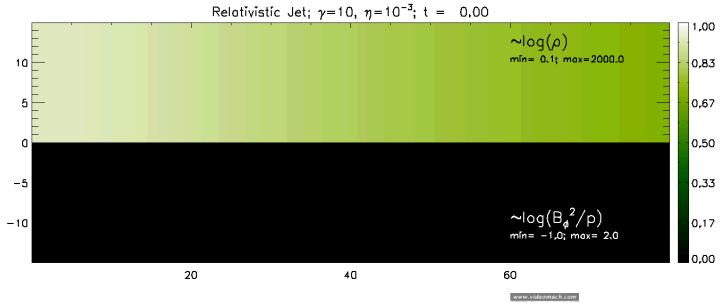

3D propagation

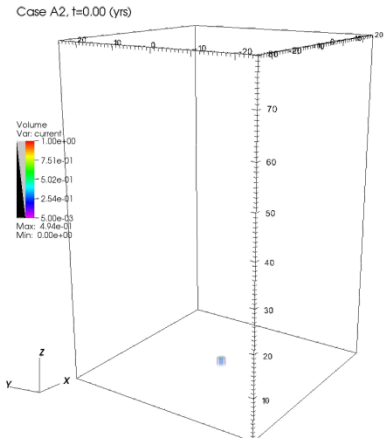

[1]Mignone et al. MNRAS (2010), 402, 7, [2]Mignone et al. MNRAS (2013), accepted

3D Simulations of Relativistic Jets

- 3D simulations by U. of Torino[1] (~ $2 \cdot 10^5$ CPU hours) confirm that the field topology is essential in determining the dynamics;

Poloidal (vertical) magnetic field:

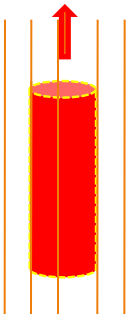

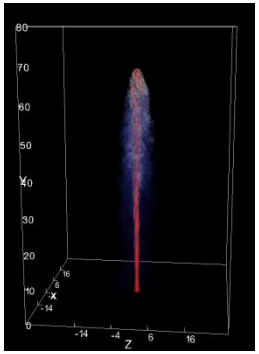

[1]Mignone et al. (MNRAS, 2009)

3D RMHD Jet
- Poloidal Field -

Grid Size:
640x1600x640

Simulation
10^5 Hours on
IBM Power 6
Cineca (Italy)
4 TB Data

Code:
PLUTO

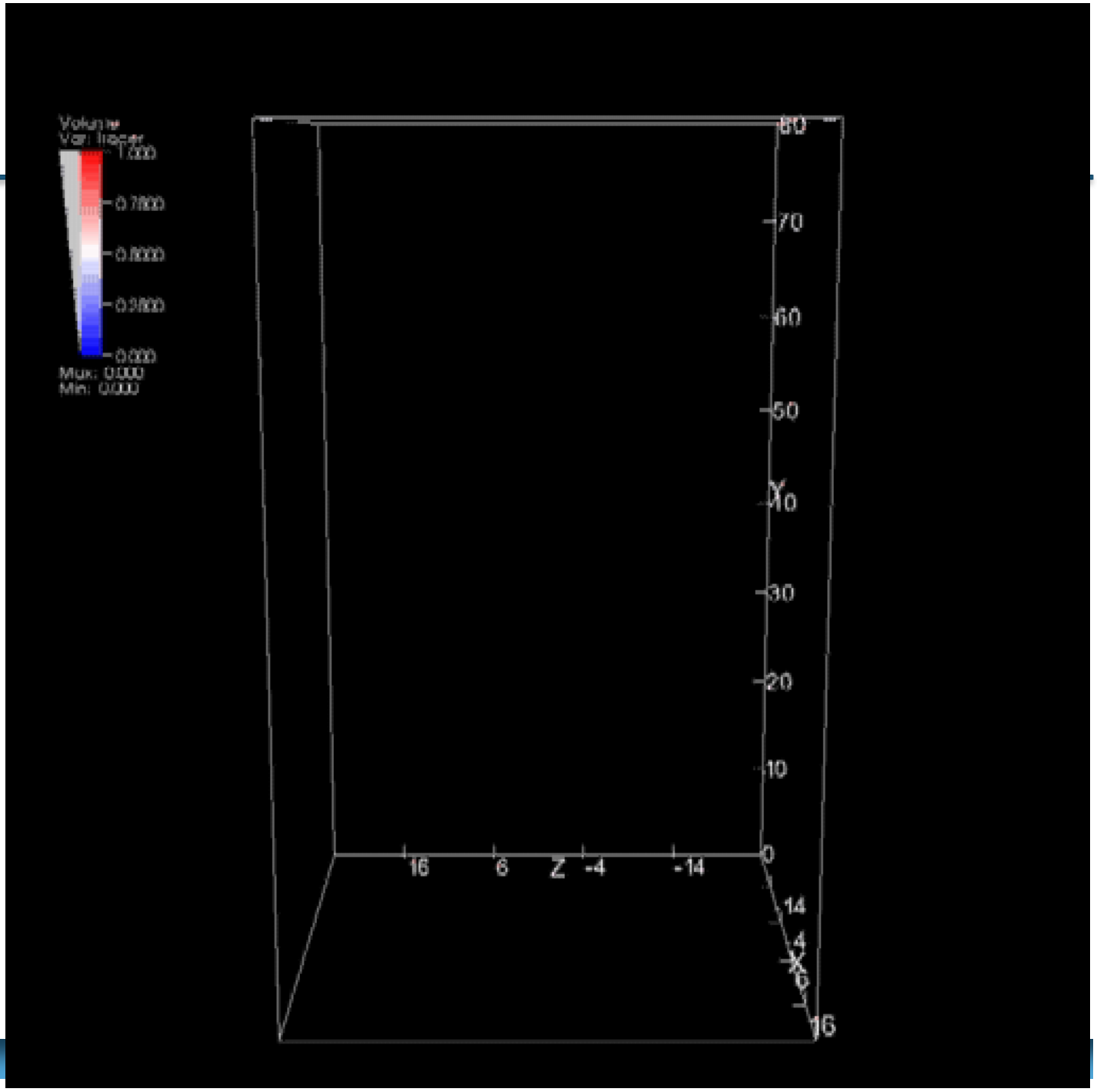

3D Simulations of Relativistic Jets

- 3D simulations by U. of Torino[1] (~ $2 \cdot 10^5$ CPU hours) confirm that the field topology is essential in determining the dynamics;

Poloidal (vertical) magnetic field:

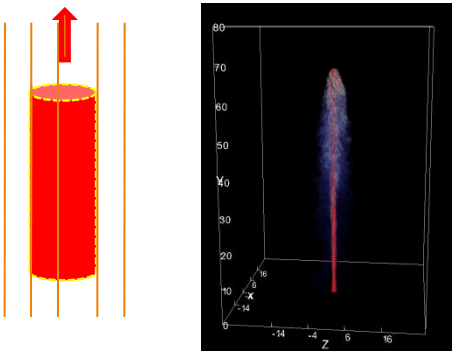

Toroidal (azimuthal) magnetic field

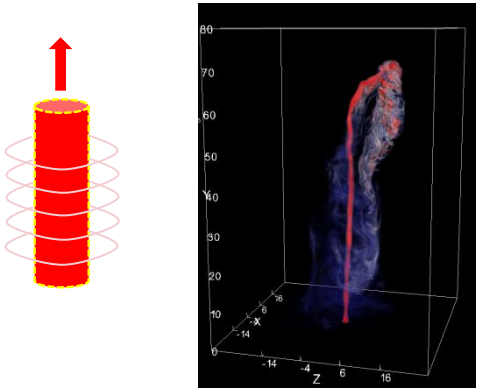

[1]Mignone et al. (MNRAS, 2009)

3D RMHD Jet
- Toroidal Field -

Grid Size:
640x1600x640

Simulation
10^5 Hours on
IBM Power 6
Cineca(Italy)
4 TB Data

Code:
PLUTO

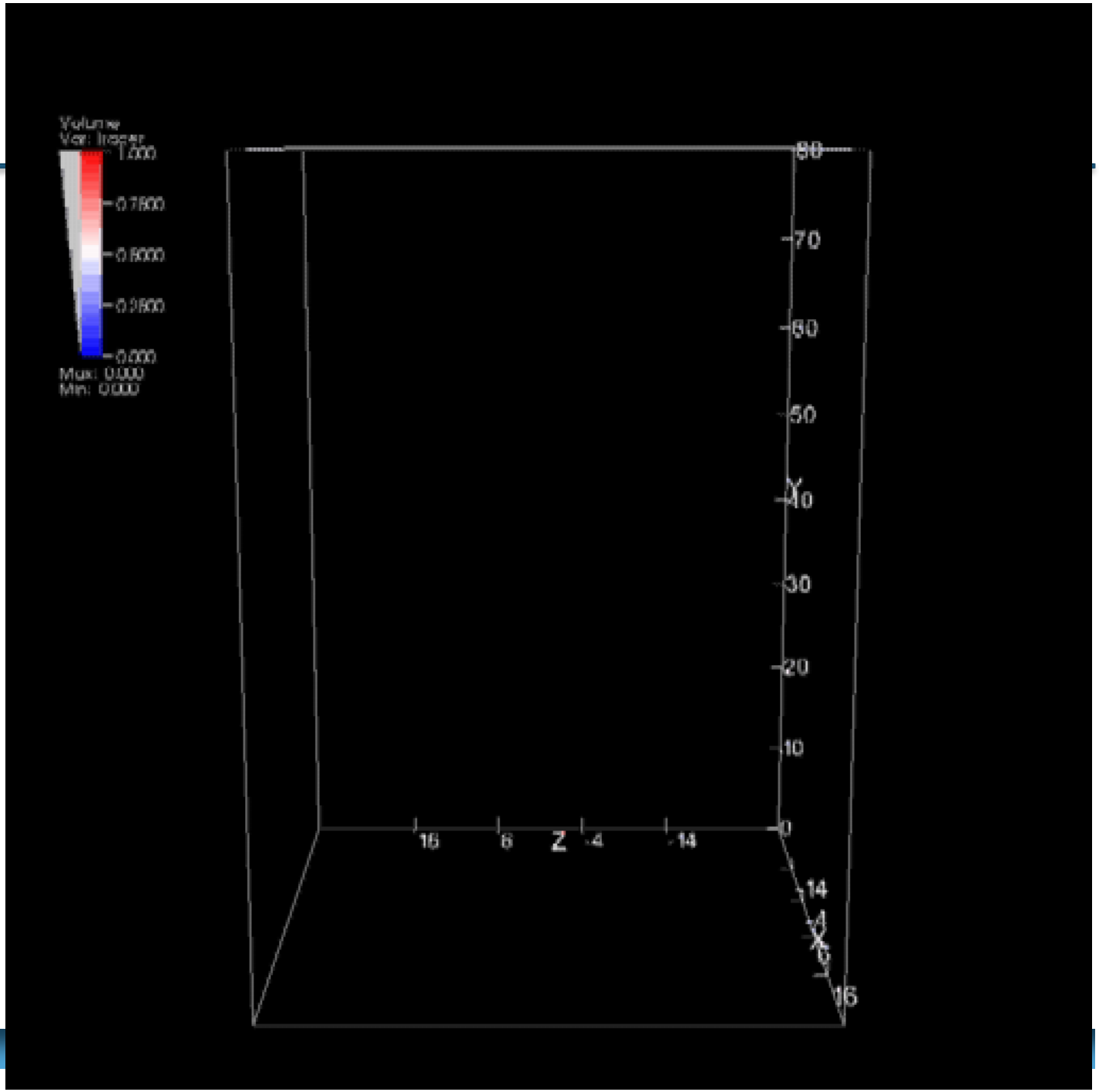

3D Simulations of Relativistic Jets

- 3D simulations by U. of Torino[1] (~ $2 \cdot 10^5$ CPU hours) confirm that the field topology is essential in determining the dynamics;

Poloidal (vertical) magnetic field:

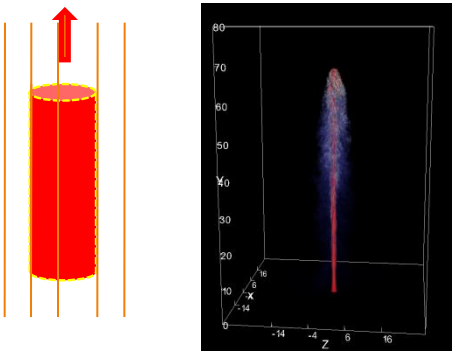

Toroidal (azimuthal) magnetic field

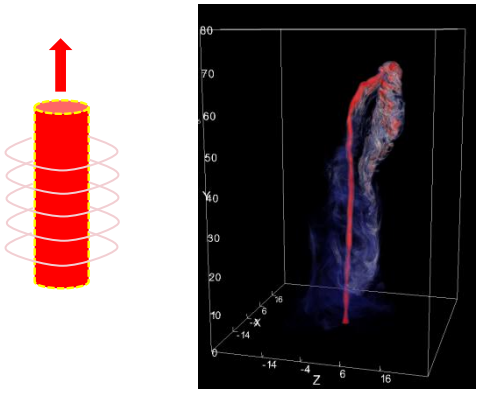

- Jet wiggling/beam deflection due to kink instabilities (m=1);
- → multiple sites where the jet impacts on the ambient forming shocks (compatible with multiple hotspots observed in several radiogalaxies);
- Backflow asymmetry replicates observational appearance of several objects.

[1]Mignone et al. (MNRAS, 2009)

Relativistic MHD jets: 2D vs 3D

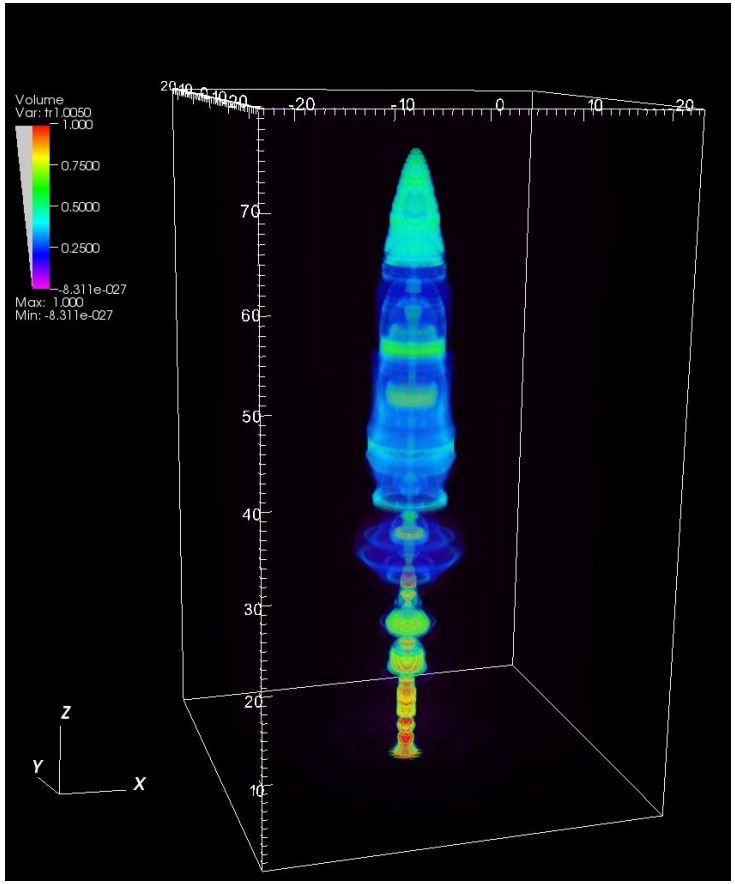

Axisym (“2.5” D)

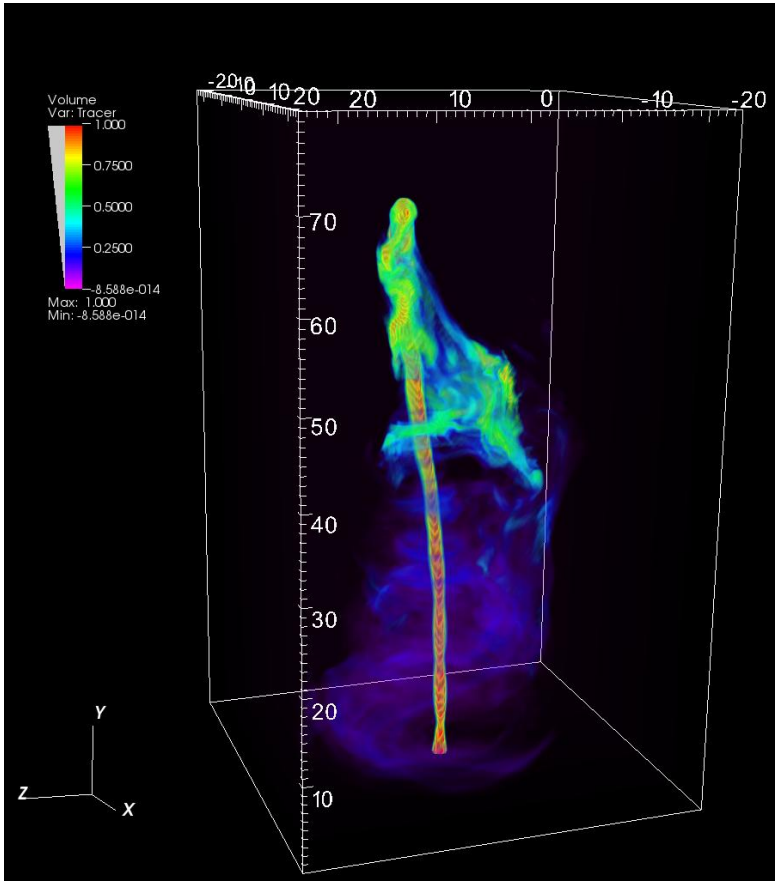

Fully 3-D

Simulation credits: The PLUTO Code

- PLUTO is modular parallel code providing a *multi-physics* as well as a *multi-algorithm* framework for the solution of conservation laws in astrophysics;

- Target: compressible, high-mach number flows with shocks in multiple spatial dimensions:
  - Compressible Euler / Navier Stokes equations;
  - Classical (ideal/resistive) Magnetohydrodynamics (MHD);
  - Special Relativistic hydro and MHD;
  - Heating/cooling processes, chemical network

- Variety of numerical methods:
  - Finite Volume / Finite Difference
  - Riemann solvers;
  - $2^{nd} - 5^{th}$ order interpolation techniques;

- Support static grid and Adaptive Mesh Refinement (AMR) computation

The PLUTO Code

- PLUTO is freely distributed at http://plutocode.ph.unito.it;
- More than 300 downloads in one year;

- References:
  - Mignone et al, Astrophys. J. Suppl. S. 170 (2007) 228. (static version)
  - Mignone et al, Astrophys. J. Suppl. S. 198 (2012) 7. (AMR version)

THE END

THANK YOU

FOR

YOUR ATTENTION